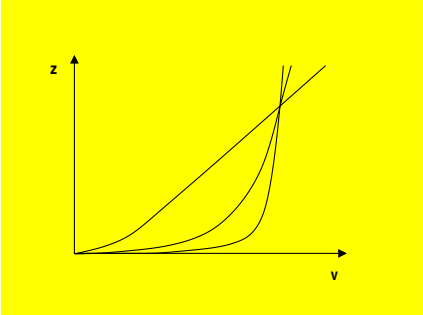

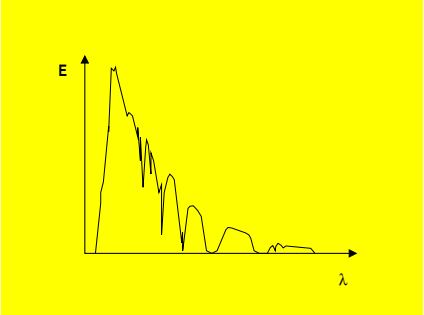

Detlev Heinemann

ENERGY METEOROLOGY

LECTURE NOTES

POSTGRADUATE PROGRAMME 'RENEWABLE ENERGY'

CARL VON OSSIETZKY UNIVERSITÄT

OLDENBURG 2002

Preface

This text includes the material presented in a one-semester course for students in the field of solar and wind energy fundamentals and applications.

It is not meant as a general introduction to atmospheric physics although it covers basic concepts of at least two fundamental fields of physics which are essential for atmospheric processes: radiation and hydrodynamics.

Moreover, the text introduces the basic meteorological knowledge necessary for the understanding of the natural constraints for using solar and wind energy resources. The material should provide the reader with the elementary physical fundamentals of atmospheric processes which make solar and wind energy resources available at the earth surface.

Based on this, methods are presented for assessing the corresponding solar and wind energy resources on different spatial and temporal scales. State-of-the-art modelling techniques for the derivation of the various quantities used for design, simulation and analysis of solar and wind energy conversion systems are introduced. Chapters dealing with instrumentation and techniques for measurements of solar radiation and wind speed conclude this introduction to basic energy meteorology.

Oldenburg, December 2002 *Detlev Heinemann*

P.S.: This text is far from being complete! Several chapters already available lack important details, other chapters - especially the more advanced - are missing at all. After completion, the text will present a state-of-the-art overview of meteorological basics needed in renewable energy as well as specific methods and applications within the field of energy meteorology.

Contents

Part I

Solar Radiation

1. Introduction

Solar radiation is the primary natural energy source of the Earth. (Other natural sources are: geothermal heat flux from the earth interior, natural terrestrial radioactivity, cosmic radiation. These are negligible!)

Solar radiation mainly emanates as electromagnetic radiation from the surface of the sun (photosphere). It is originated by several nuclear fusion processes in the interior of the sun.

The solar irradiance incident on a given plane on the earth's surface is determined by:

- sun-earth astronomy
  (physical (radiative) properties of the sun (T, ϵ), sun-earth distance)
  $\longrightarrow$ extraterrestrial solar radiant flux
- solar geometry
  (latitude, declination, solar time, azimuth and tilt angle of receiving surface)
  $\longrightarrow$ position of the sun with respect to the receiving surface
- extinction processes in the atmosphere
  (absorption and scattering by air molecules, water vapor, aerosols, clouds, ... (air mass, turbidity))
  $\longrightarrow$ available radiant flux at the surface (direct, diffuse)

These points are subject to the subsequent chapters.

2. Fundamental Physics of Solar Radiation

This chapter describes the basic aspects of the transfer of energy by electromagnetic radiation as one of three fundamental physical transfer processes. From the other elementary processes, heat conduction and convection, are convective processes of great importance for atmospheric energy transfers but will not be covered in the scope of this text.

The fundamental physical concepts and functions introduced by Planck, Kirchhoff and Stefan-Boltzmann are introduced and the electromagnetic spectrum emitted by the sun is presented. Using this framework the solar constant and the extraterrestrial radiation as a measure of the radiant flux received by the earth from the sun are calculated.

All matter emits electromagnetic radiation at all wavelengths due to its atomic and molecular agitation unless it is at a temperature of 0 K. The intensity and the spectral distribution of the radiation is solely determined by the temperature and the material properties of the emitting body (particularly of its surface). Both are described by the fundamental radiation laws of Kirchhoff and Planck.

A good approximation of intensity and spectral distribution of the radiation of a given body can be made by using the idealized concept of a black body. A perfect black body is an object that does not reflect any radiation whatever, but fully absorbs all radiation falling on it. It emits the maximum amount of energy along all wavelengths and into all directions.

2.1 Radiation Laws

Planck's law for the spectral energy density of black-body radiation at temperature T is given by

$$u_\nu(T) = \frac{8\pi h\nu^3}{c^3}\frac{1}{e^{h\nu/kT}-1} \quad [\mathrm{Wm^{-3}sr^{-1}s^2}], \tag{2.1}$$

where $k = 1.381 \cdot 10^{-23}\,\mathrm{WsK^{-1}}$ is Boltzmann's constant, $h = 6.626 \cdot 10^{-34}\,\mathrm{Ws^2}$ is Planck's constant and $c = 2.998 \cdot 10^8\ \mathrm{ms^{-1}}$ is the vacuum velocity of light.

A more practical formulation of Planck's law takes into account that the photons move isotropically with speed c, e.g. within a small solid angle. Then for the

calculation of the energy flux density of black-body radiation at temperature T into a unit solid angle as a function of frequency a factor $4\pi/c$ has to be applied and it becomes:

$$L_\nu(T) = \frac{2h\nu^3}{c^2}\frac{1}{e^{h\nu/kT}-1} \quad [\mathrm{Wm^{-2}sr^{-1}s}] \tag{2.2}$$

This expression is called the Planck function and can also be written in terms of wavelength:

$$L_\lambda(T) = \frac{2hc^2}{\lambda^5}\frac{1}{e^{hc/\lambda kT}-1} \quad [\mathrm{Wm^{-2}sr^{-1}\mu m^{-1}}],. \tag{2.3}$$

The hemispherical spectral radiant flux emerging from a unit surface (radiant exitance) then is (Fig. 2.1):

$$M_\lambda(T) = \pi L_\lambda(T) \quad [\mathrm{Wm^{-2}\mu m^{-1}}] \tag{2.4}$$

For each temperature the black-body emission approaches zero for very small and very large wavelengths. The curve for a warm black body lies above the curve for a cooler black body at each wavelength.

Approximately, the sun (more strictly, its gaseous surface) is a black-body emitter. The effective surface temperature is ~ 5780 K.

The relationship between the wavelength of a black body's maximum emission λ_m and the corresponding absolute temperature is given by Wien's displacement law which results from taking the derivative of Planck's equation:

$$\lambda_m = \frac{2897\mu\mathrm{mK}}{T}. \tag{2.5}$$

2.2 Radiant Flux Emitted by the Sun

Integration of Planck's function (Eq. 2.3) over the entire wavelength domain leads to the fundamental *Stefan-Boltzmann law*, which gives the total radiant flux density emitted by a blackbody at temperature T (emitted radiation per unit time and area):

$$M = \int_0^\infty M_\lambda(T)\,d\lambda = \pi\int_0^\infty L_\lambda(T)\,d\lambda = \sigma T^4 \tag{2.6}$$

where $\sigma = 2\pi^5k^4/15c^2h^3 = 5.67\cdot 10^{-8}\,\mathrm{Wm^{-2}K^{-4}}$ is the Stefan-Boltzmann constant.

Inserting T = 5780 K yields the radiant exitance from the sun's surface:

$$\begin{aligned} M_{sun} &= 5.67\cdot 10^{-8}\cdot 5780^4\ \mathrm{Wm^{-2}} \\ &= 6.33\cdot 10^7\ \mathrm{Wm^{-2}}. \end{aligned} \tag{2.7}$$

With $A_{sun} = 4\pi r_{sun}^2$ and $r_{sun} = 6.96 \cdot 10^8$ m, the total radiant flux emitted by the sun is:

$$\begin{aligned} \Phi_{sun} &= M_{sun} \cdot A_{sun} \\ &= 6.33 \cdot 10^7 \text{ Wm}^{-2} \cdot 4 \cdot 3.14 \cdot (6.96 \cdot 10^8 \text{ m})^2 \\ &= 3.85 \cdot 10^{26} \text{ W}. \end{aligned} \tag{2.8}$$

2.3 Solar Constant

From energy conservation principles the total radiant flux through the surface of the sun (Φ_{sun}) equals the flux through any spherical surface concentric to the sun. Especially, for a sphere with a radius $\bar{r}_{ES}$, the mean distance between sun and earth, it is (Fig. 2.3): [1]

$$4\pi r_{sun}^2 M_{sun} = 4\pi \bar{r}_{ES}^2 E_{sc} \tag{2.9}$$

The ratio $f_s = (r_{sun}/\bar{r}_{ES})^2 = 2.165 \cdot 10^{-5} \simeq 1/46200$ is called *dilution factor* and is an often used number in sun-earth astronomy.

From this, the solar radiant flux passing through a unit area at the mean distance of the earth from the sun is:

$$E_{sc} = f_s M_{sun} = 1367 \text{ Wm}^{-2} \pm 4 \text{ Wm}^{-2}. \tag{2.10}$$

[1] $\bar{r}_{ES}$ is called an astronomic unit: 1 A.U. $\simeq$ 149.6 million km.

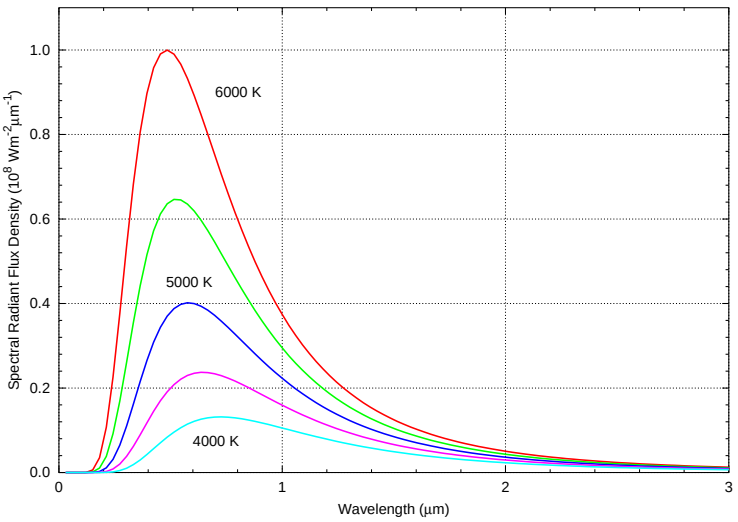

Fig. 2.1. Spectra of emitted black-body radiation for T = 6000 K to 4000 K in steps of 500 K.

E_{sc} is called the *solar constant*. This value has changed in the past as new measurement techniques (e.g. satellites) have been applied. In the literature a value of 1353 Wm^{-2} is given frequently. This value is out of date.

The solar constant is the solar radiant flux received on a surface of unit area perpendicular to the sun's direction at the average sun-earth distance outside the earth's atmosphere.

2.4 Total Solar Radiant Flux Received by the Earth

Being A_e the cross sectional area of the earth disk as seen by the sun and r_e = 6371 km the mean earth radius, it is:

$$\begin{aligned} \Phi_e &= A_e E_{sc} = \pi r_e^2 E_{sc} \\ &= 3.142 \cdot (6.371 \cdot 10^6\ \mathrm{m})^2 \cdot 1367\ \mathrm{Wm}^{-2} = 1.75 \cdot 10^{17}\ \mathrm{W}. \end{aligned} \tag{2.11}$$

Φ_e is the mean total radiant flux the earth receives from the sun. From this, the total solar energy received by the earth per year is:

$$Q_e = 5.51 \cdot 10^{24}\ \mathrm{J} = 1.53 \cdot 10^{18}\ \mathrm{kWh}. \tag{2.12}$$

Comparing this number with the annual world primary energy consumption in 1997 [2], $10.2 \cdot 10^{13}$ kWh, results in a factor of ~ 15000.

[2] BP Statistical Review of World Energy, 1998 (http://www.bp.com/bpstats)

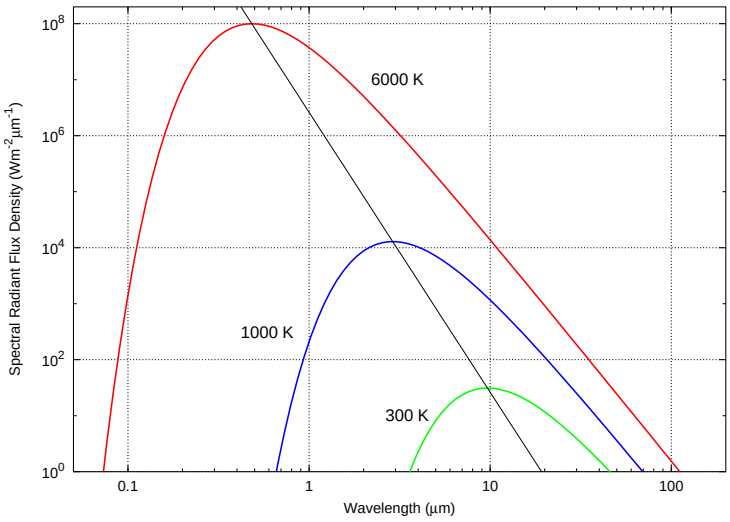

Fig. 2.2. Spectra of emitted black-body radiation for T = 6000 K (sun surface), T = 1000 K, and T = 300 K (earth surface) in a logarithmic scale. The straight line indicates the wavelength of maximum emission as a function of temperature as given by Wien's displacement law.

2.5 Extraterrestrial Radiation

The orbit of the earth around the sun is slightly elliptical with the sun at one of the foci and therefore causes a change of the sun-earth distance r_{ES} throughout the year. This variation is expressed by the eccentricity correction factor ϵ_0 (Spencer, 1971):

$$\begin{aligned}\epsilon_0 &= \left(\frac{\bar{r}_{ES}}{r_{ES}}\right)^2 \\ &\simeq 1.00011 + 0.034221\cos d + 0.00128\sin d \qquad (2.13)\\ &\quad +0.000719\cos 2d + 0.000077\sin 2d, \qquad (2.14)\end{aligned}$$

where $d = 2\pi(n-1)/365$ is the day angle in radians and n is the number of the day in the year (n = 1 on 1 January).
In most applications the simpler approximation

$$\epsilon_0 \simeq 1 + 0.033 \cdot \cos\left(\frac{360 \cdot n}{365}\right) \qquad (2.15)$$

can be used.
With this, the extraterrestrial radiation at normal incidence is given by:

$$\begin{aligned}G_{on} &= \epsilon_0 G_{sc} \\ &\simeq G_{sc}\left[1 + 0.033 \cdot \cos\left(\frac{360 \cdot n}{365}\right)\right].\end{aligned} \qquad (2.16)$$

Fig. 2.4 gives the annual variation according to Eq. 2.16.

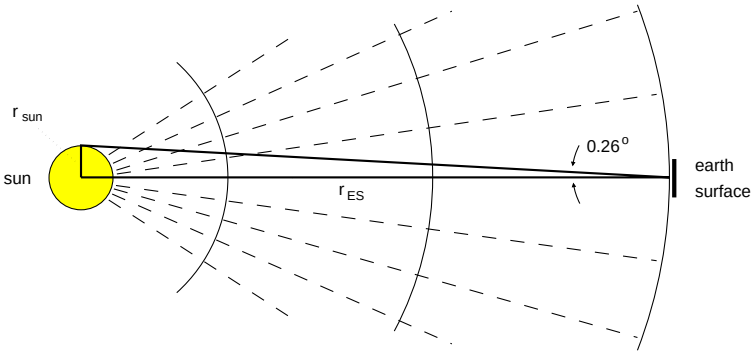

Fig. 2.3. Sun-Earth geometry.

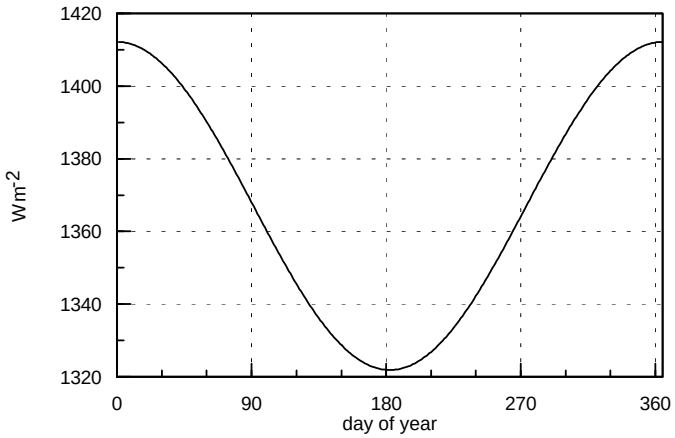

Fig. 2.4. Annual variation of the extraterrestrial irradiance at normal incidence due to the varying sun-earth distance.

3. Solar Geometry

The amount of solar radiation reaching the earth surface is affected by several influences. If the highly variable attenuation of solar radiation by the atmosphere is set aside for a moment, the specific astronomical situation of the earth's revolution around the sun and its rotation around its polar axis are the dominating effects.

As the irradiance on a plane normal to the sun's rays is exactly described by the extraterrestrial radiation, the angular displacement of the sun's position from this normal incidence has to be derived from astronomical and geographical considerations. Irradiance on any surface is than given by

$$G = G_n \cos\theta, \tag{3.1}$$

where G_n is the irradiance on a plane normal to the sun's direction and θ is the angle of incidence.

The derivation of these relationships requires the introduction of basic astronomical quantities in order to calculate the position of the sun for any location on the earth and for any time.

If second-order effects as reflection from adjacent surfaces and obstruction by neighboring structures are neglected, irradiance is fully determined by the geometric constellation of the sun and the receiver plane.:

- the position of the sun in the sky and
- the slope and orientation of the surface.

Trigonometric relationships describing the influence of the earth's revolution around the sun and the earth's rotation around its own axis ($\longrightarrow$ diurnal changes of irradiance)

Annual variations of the irradiance are mainly caused by the varying position of the polar axis with respect to the sun (in addition to the varying sun-earth distance).

3.1 Sun-Earth Astronomy

The earth revolves around the sun in a plane called *ecliptic plane*. The earth's axis (polar axis) is inclined at 23.45° (constant in time) with respect to the normal to the ecliptic plane. The same then holds for the angle between the earth's equatorial plane and the ecliptic plane.

The varying solar influence can be described by the angle between the earth's equatorial plane and the plane of its revolution around the sun. This angle is called the *solar declination* δ. Its maximum daily change is less than 0.5° (occuring at the equinoxes), so that for practical purposes a constant value for a given day can be used:

$$\delta \simeq 23.45^\circ \cdot \sin\left(\frac{360(284+n)}{365}\right). \tag{3.2}$$

The following equation gives the declination, in degrees, with an accuracy of 0.05° (Spencer, 1971):

$$\begin{aligned}\delta = {} & (0.006918 - 0.399912\cos d + 0.070257\sin d \\ & -0.006758\cos 2d + 0.000907\sin 2d) \cdot 180/\pi,\end{aligned} \tag{3.3}$$

where $d = 2\pi(n-1)/365$ is the day angle in radians.

3.2 Solar Time

Daily variations of solar radiation are usually calculated on the basis of solar time, which is defined in the following way:

A *solar day* is the time interval between two consecutive crossings of the sun's path with the local meridian. The length of this interval changes from day to day (deviation $<$ 30 sec). Only its mean value equals 24 h.

Solar noon then is the time of the crossing of the sun's path with the local meridian.

The variation of the solar day length is caused by (i) the elliptical path of the earth around the sun (Kepler's second law: The radius vector from the sun to a

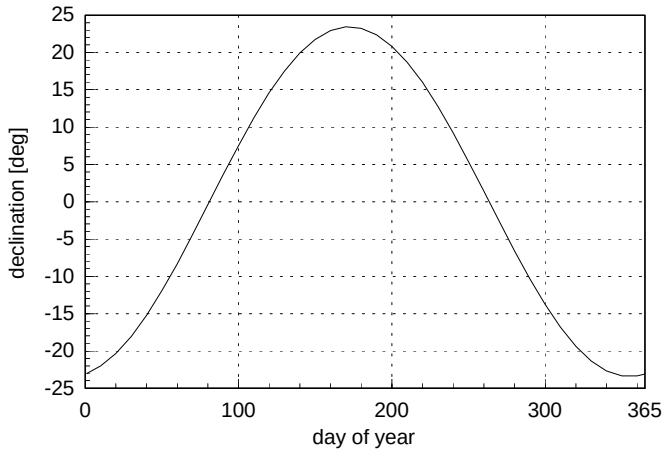

Fig. 3.1. Annual variation of the solar declination.

planet sweeps out equal areas in equal times) and (ii) the tilt of the earth's axis with respect to the ecliptic plane. This difference between the solar time and the local mean time in minutes is expressed by the empirical *equation of time* E (Fig. 3.2):

$$E \simeq 9.87 \sin 2B - 7.53 \cos B - 1.5 \sin B, \tag{3.4}$$

where $B = 360 \cdot (n - 81)/364$ in degrees.
For a higher accuracy the following formula can be used (Spencer, 1971):

$$\begin{aligned} E = {} & (0.000075 + 0.001868 \cos d - 0.032077 \sin d \\ & -0.014615 \cos 2d - 0.040849 \sin 2d) \cdot (180 \cdot 4/\pi) \end{aligned} \tag{3.5}$$

where d again is the day angle.

The maximum value of E is 16.5 minutes (for day n = 303).

Solar time differs from standard time (i.e. the time we are used to work with, determined by the time zone) due to (i) variations of the length of the solar day and (ii) a difference between the local longitude and the standard longitude of the appropriate time zone (Fig. 3.3).

$\longrightarrow$ solar time = local time + E

Note: local time $\neq$ standard time !

The local time is a function of the actual (local) longitude L_l (i.e.: same local time only on the same meridian), the standard time is a function of timezones only (corresponding to standard longitudes L_s). Usually, the standard meridians are multiples of 15° E or W of Greenwich. The standard meridian for Central Europe, for example, is 15° E (TZ = -1 from Greenwich).
The true solar time (TST or LAT) is calculated from local time (LST) using

$$\begin{aligned} LAT &= LMT + E \\ &= LST - DST + 4(L_s - L_l) + E \end{aligned} \tag{3.6}$$

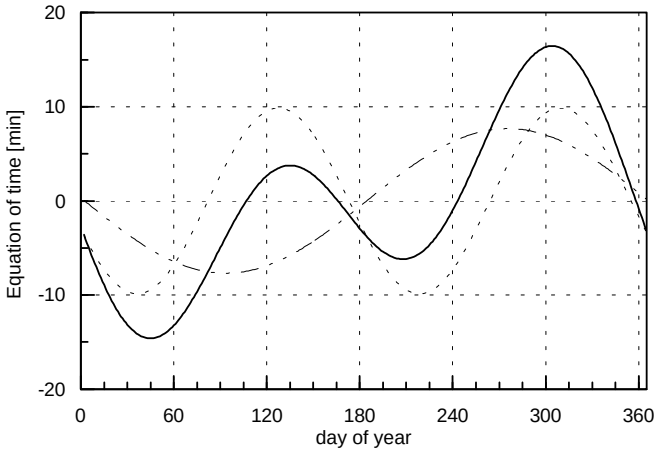

Fig. 3.2. The equation of time.

where DST = 1 hour during daylight saving time and = 0 otherwise.

Example: Calculation of the local time at solar noon for Oldenburg, October 15. The local longitude is 8.2° East (= - 8.2°), the standard longitude is 15° East (CET).

$$\begin{aligned} LST &= LAT + DST - 4(L_s - L_l) - E \\ &= 12:00 + 1 - 4(-15 - (-8.2)) - 14 \\ &= 13:00 + 0:27 - 0:14 \\ &= 13:13. \end{aligned}$$

The *hour angle* ω is a quantity which describes the solar time in trigonometric relationships. It equals the angular displacement of the sun from the local meridian due to the rotation of the earth. One hour corresponds to an angle of 15° (360°/24h). The morning hours are negative and the afternoon hours are positive by convention. At solar noon ω equals 0°.

3.3 Position of the Sun

To calculate the irradiance on any plane the position of the sun with respect to that plane (precisely: to the normal to that plane) must be known. The sun's position in the sky hemisphere can be completely described by two quantities (Fig. 3.4):
*3mm – solar altitude α (elevation above horizon)
– solar azimuth ψ
The sun's altitude is given by spherical trigonometry (with geographical latitude ϕ):

$$\sin\alpha = \sin\delta\sin\phi + \cos\delta\cos\phi\cos\omega \tag{3.7}$$

The solar azimuth is given by:

$$\cos\psi = \frac{\sin\alpha\sin\phi - \sin\delta}{\cos\alpha\cos\phi} \tag{3.8}$$

The quantity describing the angle between the incoming solar beam radiation and the normal to the receiving surface is the angle of incidence θ (Fig. 3.4).

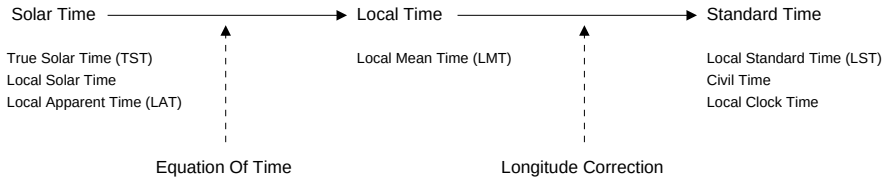

Fig. 3.3. Commonly used terms of time and their relationship.

This angle depends on
- geographical location (latitude)
- time of year (declination), time of day (hour angle)
- orientation of the plane (slope β, surface azimuth γ):

$$\theta = f(\phi, \delta, \omega, \beta, \gamma). \tag{3.9}$$

For its calculation, two additional angles have to be introduced: The slope angle β between the collector plane and the horizontal surface which varies between 0° for a horizontal plane and 90° for a vertical plane. The surface azimuth angle γ as the deviation of the normal of the plane from the local meridian. γ is counted clockwise from N where its value is 0° (thus for S it is 180°) on both hemispheres. Note that in the literature often a value of 180° for an orientation towards the equator is used! Then it is:

$$\begin{aligned}\cos\theta = &\sin\delta\,(\sin\phi\cos\beta + \cos\phi\sin\beta\cos\gamma)\\ &+ \cos\delta\cos\omega\,(\cos\phi\cos\beta - \sin\phi\sin\beta\cos\gamma)\\ &- \cos\delta\sin\beta\sin\gamma\sin\omega)\end{aligned} \tag{3.10}$$

In case of some special situations simplified expressions can be given:

- Horizontal surfaces: $\beta = 0°(i.e., \cos\beta = 1, \sin\beta = 0)$

  $$\cos\theta = \sin\delta\sin\phi + \cos\delta\cos\phi\cos\omega \tag{3.11}$$

  For horizontal surfaces θ equals the zenith angle θ_z (see Fig.3.4).
  The $90°$ complement of the zenith angle is the solar elevation angle α (solar altitude).
- Vertical surfaces facing towards the equator: $\beta = 90°, \gamma = 180°$ for the northern hemisphere and $\gamma = 0°$ for the southern hemisphere

  $$\cos\theta = -\sin\delta\cos\phi + \cos\delta\sin\phi\cos\omega \tag{3.12}$$

- Inclined surfaces facing towards the equator with a tilt angle equal to the absolute value of the latitude (northern hemisphere: $\beta = \phi$, $\gamma = 180°$; southern hemisphere, $\beta = -\phi$, $\gamma = 0°$):

  $$\cos\theta = \cos\delta\cos\omega \tag{3.13}$$

  For solar noon ($\omega = 0°$) it is: $\theta = |\delta|$.
- Sunrise and sunset: $\theta_z = 90°$

  $$\sin\delta\sin\phi = -\cos\delta\cos\phi\cos\omega$$

  In this case, the sunset hour angle ω_{ss} is:

  $$\cos\omega_{ss} = -\frac{\sin\delta\sin\phi}{\cos\delta\cos\phi} = -\tan\delta\tan\phi$$

Example: Daylength for winter solstice (21 December) in Oldenburg, Germany:
$\phi = +53.2°, \delta = -23.45°$
$\cos\omega_{ss} = -\tan(53.2°)\tan(-23.45°) = +0.58$
$\omega_{ss} = -54.56°$
The angle between sunrise and sunset then is $2|\omega_{ss}| = 109.12°$ resulting in a theoretical sunshine duration of $109.12°/15° = 7.27$ hours for that particular day.

3.4 Example: Extraterrestrial Radiation on a Horizontal Surface

- Instantaneous value:

$$\begin{aligned} G_o &= G_{on}\cos\theta_z \\ &\simeq G_{sc}\left\{1 + 0.033\cdot\cos\left(\frac{360\cdot n}{365}\right)\right\}\cos\theta_z \end{aligned} \tag{3.14}$$

- For a time period (t_1,t_2) with corresponding hour angles ω_1 and ω_2 Eq. 3.11 and integration gives:

$$\begin{aligned} I_o &= \int_{t_1}^{t_2} G_o dt = \int_{\omega_1}^{\omega_2} G_o \frac{12\cdot 3600}{\pi} d\omega \\ &= \frac{12\cdot 3600}{\pi} G_{sc}\left\{1 + 0.033\cos\left(\frac{360\cdot n}{365}\right)\right\}\cdot \\ &\quad \cdot\left(\cos\phi\cos\delta(\sin\omega_2 - \sin\omega_1) + \frac{\pi(\omega_2-\omega_1)}{180}\sin\phi\sin\delta\right), \end{aligned}$$

  where $dt = (24\text{h}/2\pi)d\omega$. I_o is in Jm^{-2}.
- Similarly, the daily extraterrestrial radiation is given in Jm^{-2}:

$$\begin{aligned} H_o &= \int_{-\omega_{ss}}^{\omega_{ss}} G_o dt \\ &= \frac{24\cdot 3600}{\pi} G_{sc}\left\{1 + 0.033\cos\left(\frac{360\cdot n}{365}\right)\right\}\cdot \\ &\quad \cdot\left(\cos\phi\cos\delta\sin\omega_{ss} + \frac{\pi\omega_{ss}}{180}\sin\phi\sin\delta\right) \end{aligned}$$

  where n is again the number of the day in the year and ω_{ss} is in degrees.

Fig. 3.4. Zenith angle θ_z, slope β, surface azimuth angle γ and solar azimuth angle ψ for a tilted surface.

4. Interaction of Solar Radiation with the Atmosphere

In the previous chapters only the extraterrestrial radiation has been considered; i.e., the radiative transfer through the atmosphere was not influenced by the atmosphere.
$\longrightarrow$ deterministic radiation calculation; only solar geometry

As solar radiation passes through the earth's atmosphere, some of it is absorbed or scattered by air molecules, water vapor, aerosols, and clouds. The solar radiation that passes through directly to the earth's surface is called direct solar radiation. The radiation that has been scattered out of the direct beam is called diffuse solar radiation. The direct component of sunlight and the diffuse component of skylight falling together on a horizontal surface make up global solar radiation.

Determining the irradiance at the surface requires knowledge of the influence of the atmosphere. Looking at the different components in the atmosphere which could influence the radiation transfer, mainly two groups have to be considered: The gaseous molecules of dry air which are uniformly mixed both in the horizontal and in the vertical below heights of 80 km and the highly variable amounts of water vapor (H_2O) and aerosol particles. Water vapor is present in a range between 0 and 4 per cent of the humid atmosphere with a vertical profile showing a strong decrease of concentration with height.

Finally, the liquid and solid water contained in clouds has to be considered as a main attenuator of solar radiation in the atmosphere.

Table 4.1. Composition of the dry atmosphere by volume (ppm = parts per million).

Nitrogen	78.08 %
Oxygen	20.95 %
Argon	0.93 %
Carbon Dioxide	350 ppm
Neon	18 ppm
Helium	5 ppm
Krypton	1 ppm
Hydrogen	0.5 ppm
Ozone	0.05-12 ppm (variable)

The main processes for the extinction of solar radiation passing through the atmosphere are:

– absorption by ozone

- absorption by uniformly mixed gases (O_2, CO_2)
- absorption by water vapor
- scattering by molecules of the air
- extinction by aerosol particles
- extinction by clouds (high cirrus clouds, thick clouds)

absorption:
solar radiation is converted to heat by atmospheric constituents; this energy is lost!
strongly wavelength dependent; occurring in several characteristic wavelength bands

scattering:
scattering changes direction and wavelength of the radiation; no conversion!
solar radiation is scattered partly back to space!
scattering is strongly wavelength dependent: Rayleigh-scattering ($d < \lambda$) due to molecules follows an λ^{-4}-law, Mie-scattering ($d \sim \lambda$) due to aerosols is approximately $\lambda^{-1.5}$-dependent.

Scattering is a process whereby light is actually absorbed by a particle and then emitted in another direction. Scattering particles can be air molecules, dust particles, water droplets, gases or particulates, which scatter incoming sunlight (or moonlight) in all directions. Scattering can also be viewed as a reflection off of the scatterer.

Selective scattering (or Rayleigh scattering) occurs when certain particles are more effective at scattering a particular wavelength of light. Air molecules, like oxygen and nitrogen for example, are small in size and thus more effective at scattering shorter wavelengths of light (blue and violet). The selective scattering by air molecules is responsible for producing the blue skies we often see on a clear sunny day.

Another type of scattering (called Mie Scattering) is responsible for the white appearance of clouds. Mie scattering occurs when the wavelengths of visible light are more or less equally scattered.

Rayleigh scattering models the scattering for extremely small particles such as molecules of the air. The amount of scattered light depends on the incident light angle. It is largest when the incident light is parallel or anti-parallel to the viewing direction and smallest when the incident light is perpendicular to the viewing direction.

The angular distribution of the scattered radiation is given by the Rayleigh scattering phase function for unpolarized incident radiation (Fig. 4.1):

$$P(\psi) = \frac{3}{4}(1 + \cos^2 \psi) \tag{4.1}$$

$P(\psi)$ is a non-dimensional parameter and is normalized to unity, i.e., it has the property that

$$\frac{1}{4\pi} \int^2 \pi_0 \int_0^{\pi} \sin \psi d\psi d\theta = 1.q \tag{4.2}$$

Mie scattering is used for relatively small particles such as minuscule water droplets of fog, cloud particles, and particles responsible for the polluted sky. In

this model the scattering is extremely directional in the forward direction i. e. the amount of scattered light is largest when the incident light is anti-parallel to the viewing direction (the light goes directly to the viewer). It is smallest when the incident light is parallel to the viewing direction.

The Henyey-Greenstein scattering is based on an analytical function and can be used to model a large variety of different scattering types. The function models an ellipse with a given eccentricity e. An eccentricity value of zero defines isotropic scattering while positive values lead to scattering in the direction of the light and negative values lead to scattering in the opposite direction of the light. Larger values of e (or smaller values in the negative case) increase the directional property of the scattering.

These extinction processes depend on

– amount of interacting molecules and particles (turbidity)
– path length of the radiation through the atmosphere.

⟶ concept of relative air mass
⟶ different extinction for different zenith angles even for unchanging atmosphere

Table 4.2. Contribution of atmospheric constituents to total extinction (○ = weak, ● = intermediate, ●● = strong).

	absorption	scattering
Ozone (O_3)	●	○
O_2, CO_2	●	○
all molecules	○	●●
water vapor	●●	○
aerosols	●	●●
clouds	●	●

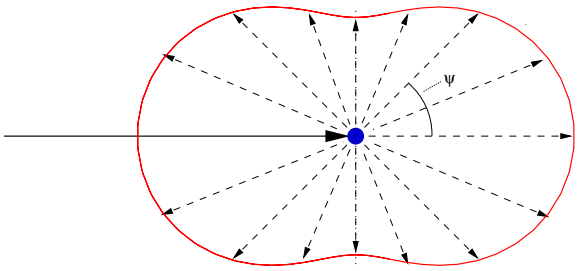

Fig. 4.1. Rayleigh scattering phase function for unpolarized incident radiation as a function of the scattering angle.

4.1 Relative Air Mass

For an assessment of extinction processes in the atmosphere it is necessary to know the total mass or 'optical path' of atmosphere which the beam traverses on its way to the surface (or the level in question).

The relative path length of direct solar beam radiance through the atmosphere is given by the ratio between the vertical optical path m and the actual optical path m_s of the solar beam. It can be described as a function of the zenith angle θ_z only:

$$\frac{m_s}{m} = \frac{1}{\cos\theta_z} = \sec\theta_z = m_r. \tag{4.3}$$

The quantity m_r is known as the *relative air mass*. In solar energy for m_r commonly AM is used (Fig. 4.3).
Eq. (4.3) is strictly valid only for a plane parallel atmosphere. In a real, spherical atmosphere with refraction the relative air mass AM is limited to about 36.5.

More accurate values for the relative air mass at standard pressure can be obtained from (Kasten, 1966):

$$m_r = \left[\cos\theta_z + 0.15(93.885 - \theta_z)^{-1.253}\right]^{-1}. \tag{4.4}$$

Definition of relative air mass for a horizontal homogeneous atmosphere:

$$m_r = \frac{\int_0^\infty \rho ds}{\int_0^\infty \rho dz}. \tag{4.5}$$

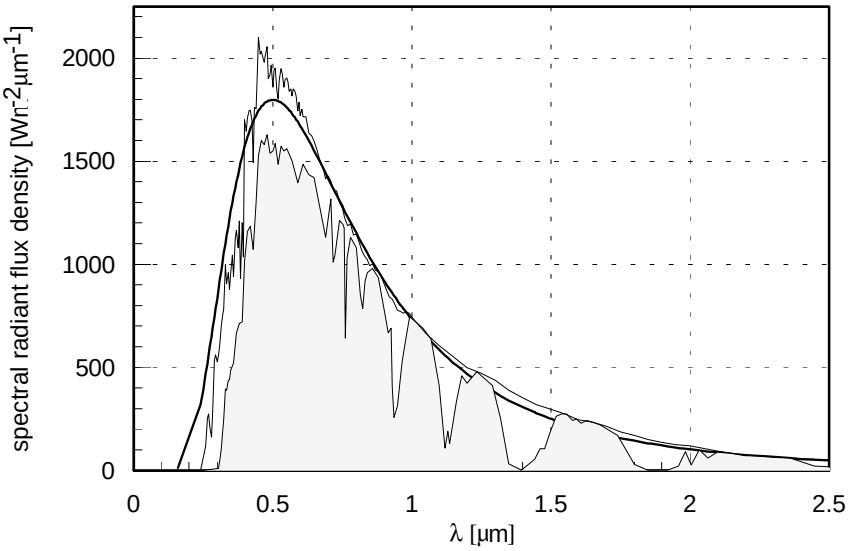

Fig. 4.2. Planck spectrum for a black body at T=5780 K (thick curve) and observed solar spectra at the top of the atmosphere (extraterrestrial, thin curve) and at the Earth surface (grey area).

By definition, the case of extraterrestrial radiation (i.e., no air mass at all) is described by AM 0.

Note: AM 1.5 is commonly used as a reference air mass in data sheets of photovoltaic modules.

4.2 Spectral Irradiance

- shift of spectrum
- spectra for clear sky
- absorption of atmospheric components

4.3 Clearness Index

The standard spectra in Chapter 4.2 apply for cloudless (i.e. clear) skies only. Thus, approximations concerning the incoming radiation are possible when geometry and atmospheric turbidity (amount of water vapor, aerosols) are known.

But: Most of the reduction in irradiance is due to clouds!
$\longrightarrow$ a quantity describing this overall reduction is the *clearness index*:

$$k_t = \frac{\int G dt}{\int G_o dt}. \tag{4.6}$$

normalization of global irradiance by corresponding extraterrestrial radiation value $\longrightarrow$ eliminating seasonal trend

k_t relates the global radiation to the extraterrestrial radiation and therefore gives a dimensionless number giving the percentage of the reduction of extraterrestrial radiation due to absorption and scattering by air molecules, aerosols, water vapour and clouds.

Convention: k_t is commonly used in a generic sense as well as for hourly values. For daily and monthly values K_t and $\bar{K}_t$ are used, respectively.

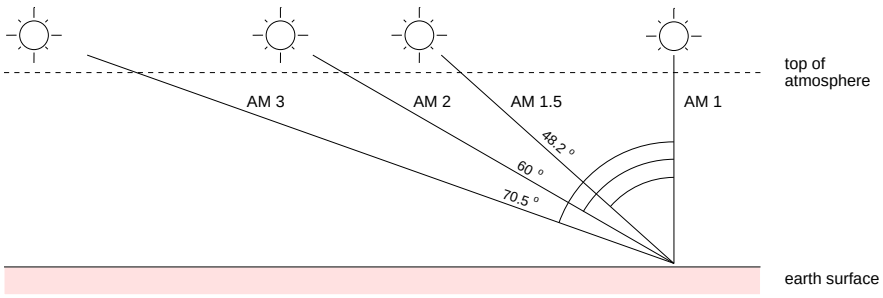

Fig. 4.3. Relative air mass and corresponding zenith angles in a plane parallel atmosphere.

The clearness index eliminates the influence of the zenith angle θ_z (daily and seasonal variation) and therefore characterizes the solar radiation climate at a particular location. Several additional quantities in solar meteorology are described as a function of the clearness index.

Table 4.3. Monthly and annual mean values of $\bar{K}_t$.

month	latitude	J	F	M	A	M	J	J	A	S	O	N	D	annual
Bergen	60.4° N	.21	.30	.36	.42	.41	.43	.38	.40	.32	.30	.23	.20	.33
Oldenburg	53.1° N	.25	.32	.37	.41	.42	.44	.41	.45	.40	.34	.28	.23	.36
Freiburg	48.0° N	.36	.39	.42	.47	.47	.49	.51	.48	.50	.43	.35	.34	.43
Carpentras	44.1° N	.44	.49	.52	.57	.57	.61	.67	.63	.57	.55	.47	.46	.55
Almeria	36.8° N	.56	.56	.52	.59	.60	.62	.66	.64	.60	.58	.56	.58	.59
Pretoria	27.0° S	.61	.55	.58	.61	.65	.69	.54	.68	.65	.59	.58	.57	.61

To eliminate also the influence of the increasing air mass with increasing zenith angle frequently the clear sky index k_t^* is used:
In this case, a standard clear sky radiation has to be considered for comparison. For AM 1.5 with given concentrations of water vapor and ozone, these values are tabulated in a spectrally resolved form.

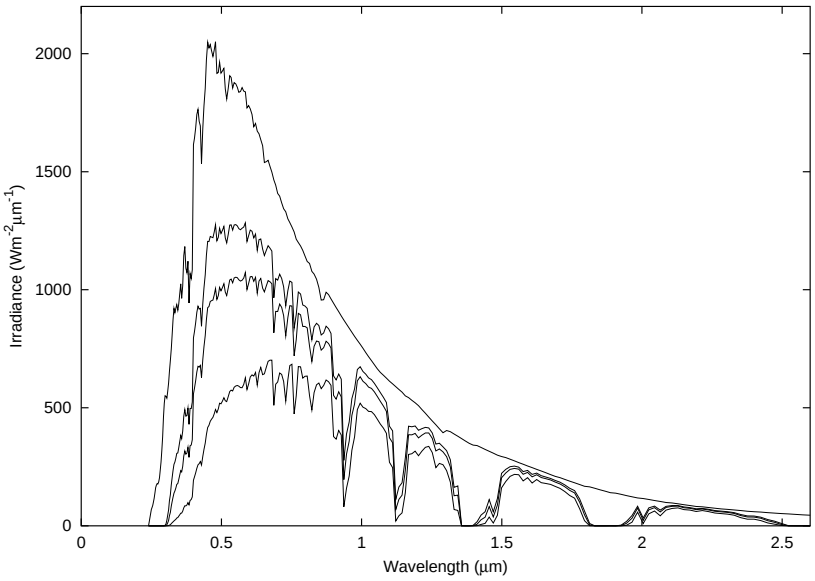

Fig. 4.4. Spectral direct normal irradiance for a clear atmosphere. different values of the atmosheric air mass (from top: AM0, AM1, AM1.5, AM3). Spectra are calculated with SBDART using a subarctic summer atmosphere (1.42 gm^{-3} water vapour, 23 km visibility).

Figure: Extraterrestrial radiation G_o, global radiation G, clearness index k_t and clear sky index k_t^* for site xxx, date yyy.

4.4 Irradiance under Clear and Cloudy Skies

4.5 Radiance Distribution on the Sky Hemisphere

4.6 Effects of Clouds and Aerosols on Solar Radiation

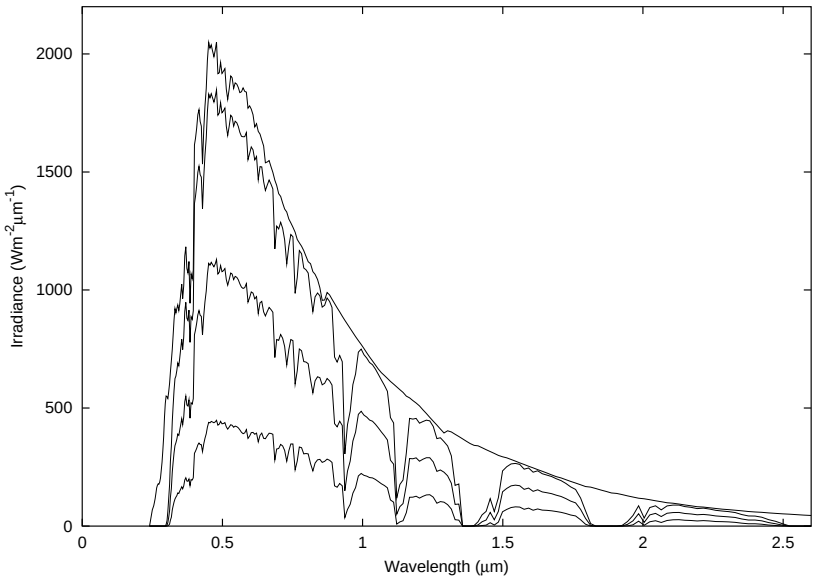

Fig. 4.5. Spectral global irradiance on a horizontal surface for a clear atmosphere and different values of the atmospheric air mass (from top: AM0, AM1, AM1.5, AM3). The corresponding total global irradiances are 1367, 1083, 669 and 276 Wm-2, respectively. Spectra are calculated with SBDART using a subarctic summer atmosphere (1.42 gm^{-3} water vapor, 23 km visibility).

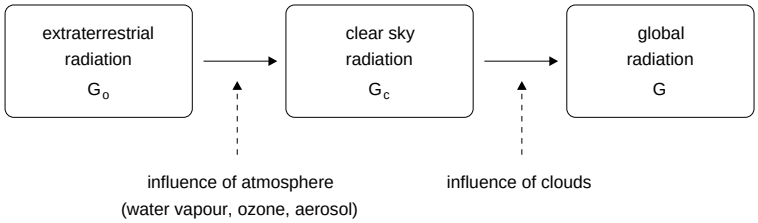
extraterrestrial
radiation
G_o
clear sky
radiation
G_c
global
radiation
G
influence of atmosphere
(water vapour, ozone, aerosol)
influence of clouds

Fig. 4.6. .

5. Radiation Climatology

If the radiant flux which the Earth is receiving permanently from the sun is distributed over the whole earth surface, the result is an radiant flux density of 342 Wm^{-2} (one quarter of the solar constant) as average extraterrestrial radiation.

The long-term, globally averaged energy balance of the earth-atmosphere system is shown in Fig. 5.2. To maintain thermal equilibrium (i.e.: constant long term average temperature), the incoming solar radiation must be balanced on average by an equal amount of radiant energy leaving the atmosphere into space. This is achieved by the reflection of shortwave solar radiation by the surface and the atmosphere as well as by longwave (infrared) absorption and emission of radiation by the surface and atmospheric constituents. The dominant role of clouds in shortwave reflection and longwave emission is very obvious. On average, only 52 per cent of the incoming radiation reaches the surface and thus is available for conversion in solar energy devices.

Only 52 % of the extraterrestrial radiation reaches the earth's surface , i.e. 178 Wm^{-2}, this gives the mean global radiation.

Long term mean solar radiation: $90 < G < 250$ Wm^{-2} (extremely influenced by mean local cloudiness)

From the global radiation budget, it can be concluded:

– total radiation reaching the ground is decreased.

– radiation is scattered off the sun direction

– diffuse radiation: radiation reaching the ground from other directions than the sun's direction

– direct radiation: radiation reaching the ground from the sun's direction (angle of $\sim 0.5\ ^\circ$)

Approximately, it is:

$\sim$ 30 % of incoming radiation is reflected back into space (by atmosphere, clouds and

surface),

$\sim$ 20 % is absorbed in the atmosphere,

$\sim$ 50 % is absorbed by the earth surface.

Variability in time

– year-to-year, mostly non-deterministic

– seasonal (high latitudes!), variation of G_o, seasonal variation of cloud amount

– daily, highly deterministic

– short term fluctuations (clouds), highly stochastic

and space
- latitude
- local climate (maritime, continental)

long-term global mean: $\sim$ 185 Wm^{-2} = 5.8 $GJm^{-2}a^{-1}$
= 1.6 MWh $m^{-2}a^{-1}$
= 4.4 kWh $m^{-2}d^{-1}$

seasonal variations: important for system layout!
geographical variations: contrast between different latitudes!

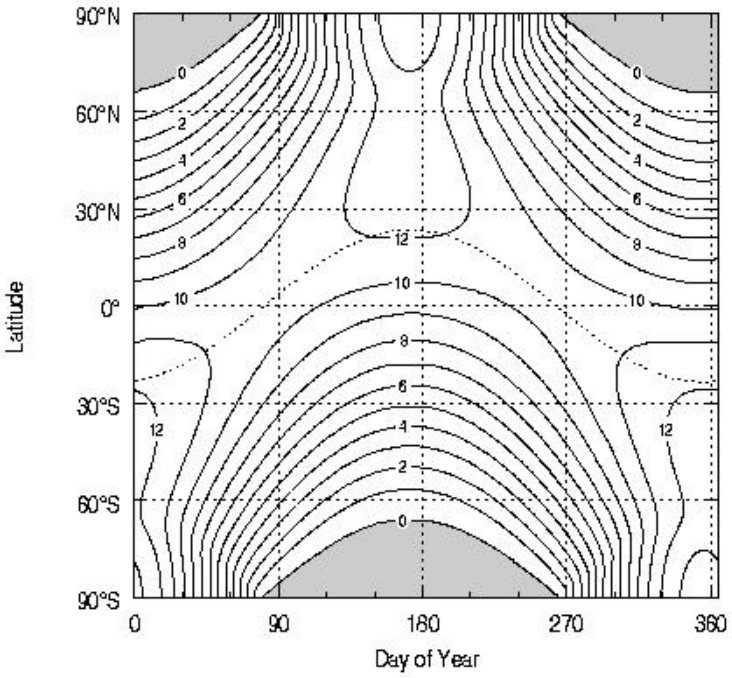

Fig. 5.1. Average daily extraterrestrial radiation on a horizontal surface as function of season and latitude.

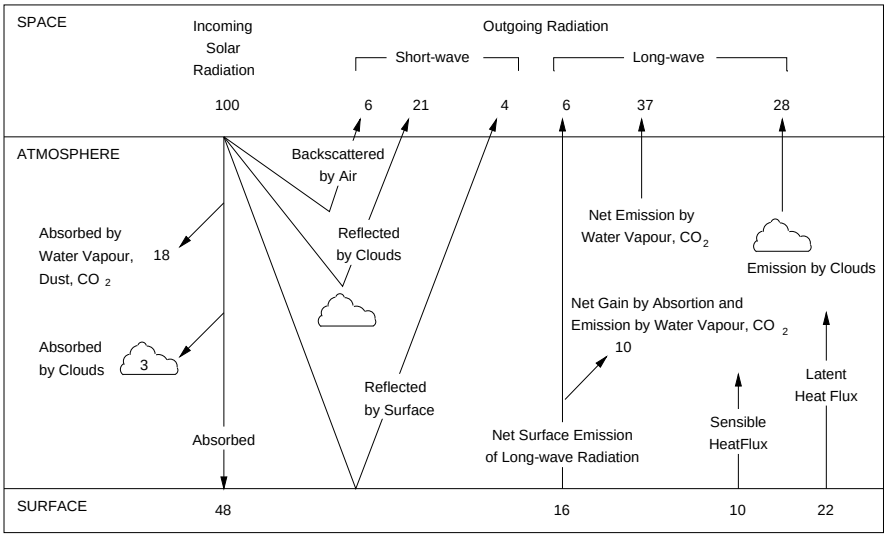

Fig. 5.2. Global mean energy budget of the earth-atmosphere system in percent of the mean solar input. 100 % = 342 Wm^{-2}.

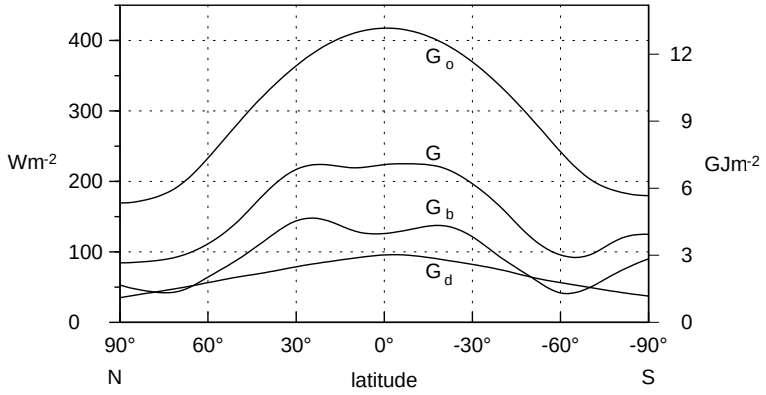

Fig. 5.3. Mean meridional profile of extraterrestrial radiation G_o, global radiation G, direct radiation G_b and diffuse radiation G_d on a horizontal surface. The scales are average irradiance (left, in Wm^{-2}) and annual solar radiation (right, in GJm^{-2}).

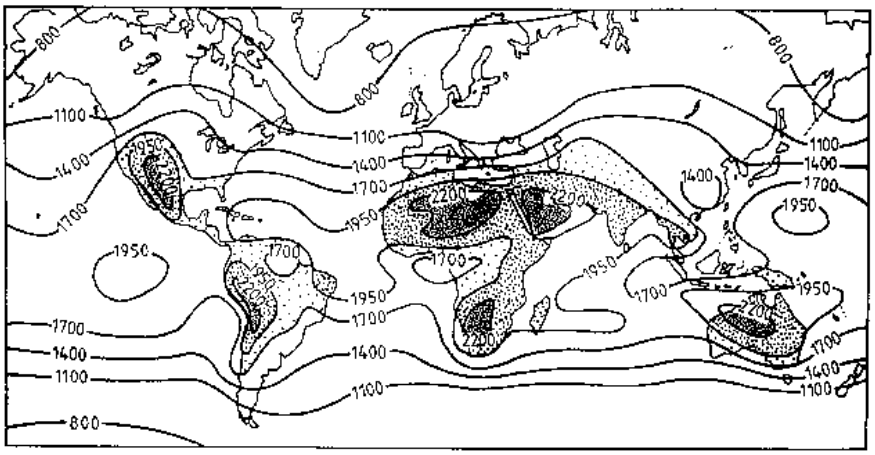

Fig. 5.4. Global distribution of annual average solar radiation (in kWhm^{-2}).

6. Solar Irradiance Modelling

Since most solar energy conversion systems are installed in a non-horizontal position, irradiance data for tilted surfaces are in great demand for solar energy research and applications.

Available solar radiation data typically consists of global horizontal data only. To yield estimates of the irradiance on tilted surfaces, these data often have to be modelled from available recordings of horizontal irradiation.

$\longrightarrow$ We need conversion models for estimating the irradiance on inclined planes.

It is current practice for evaluating the irradiation on a tilted surface to decompose the solar radiation into the components direct beam, sky diffuse and ground-reflected radiation:

$$G_t = G_{bt} + G_{dt} + G_{rt}, \tag{6.1}$$

where the indices denote tilted (t), beam (b), diffuse (d) and reflected (r) radiation, respectively.
The components then are treated separately (Fig. 6.1).

The models generally differ in the treatment of the diffuse radiation component. The representation of the distribution of radiance in the sky hemisphere is difficult. Assumptions used to describe it are main causes of errors in these models.

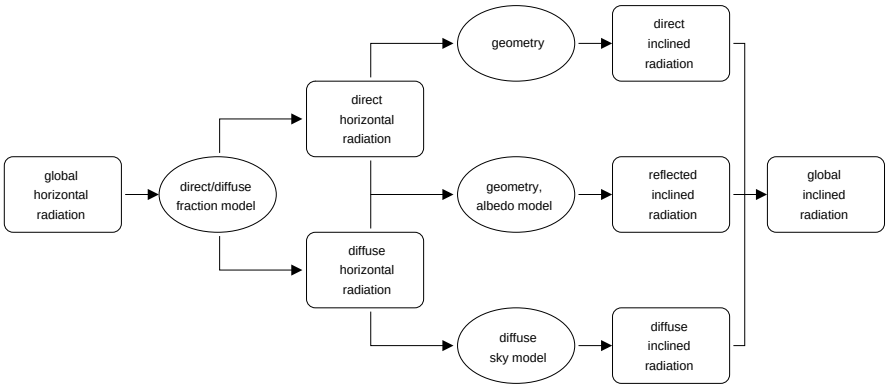

Fig. 6.1. Conversion steps for estimating global radiation on tilted surfaces from global horizontal radiation.

The modelling of direct irradiance is straightforward and identical in all models (more difficult only for time integrated values).

Ground-reflected radiation: Also difficult to estimate, but of lesser impact due to absolute lower values (only in certain circumstances of higher importance).

Requirement of knowledge of different radiation components (diffuse and direct)
Components have to be inferred from available data (usually only global)
$\longrightarrow$ Need for additional model for the diffuse/direct fractions of global radiation

6.1 Direct Radiation Component

$$G_{bt} = G_{bn} \cos\theta. \tag{6.2}$$

With $G_b = G_{bn} \cos\theta_z$ it is:

$$G_{bt} = G_b \frac{\cos\theta}{\cos\theta_z}. \tag{6.3}$$

In the literature, the ratio $\cos\theta/\cos\theta_z$ often is referred to as the geometric factor R_b.

To force the application of Eq. 6.3 to realistic cases, in computer algorithms $\cos\theta$ should be replaced by $\max(0, \cos\theta)$.

6.2 Ground-Reflected Radiation Component

Assumption: Ground reflects irradiation isotropically:

$$G_{rt} = G\rho \, \frac{1 - \cos\beta}{2}, \tag{6.4}$$

where $\rho = G_r/G$ is the albedo (reflectance) of the surface.

Important: Appropriate albedo (variations in time, snow!),
Variation in albedo with zenith angle
Second order: anisotropic effects

Modifications are only necessary when strong directional variations in reflectance or local obstructions to the horizon occur.

6.3 Diffuse Radiation Component

Different sky conditions:
- overcast: isotropic distribution is good approximation
- broken cloudiness: very difficult, largest variations
- clear sky: anisotropic effects

Plot: Hay and McKay

Table 6.1. Albedo values for selected surfaces (average values for the solar spectral range).

grassland	0.15 - 0.35
forest	0.10 - 0.25
desert	0.25 - 0.30
dry sand	0.2 - 0.4
soils	0.05 - 0.20
water (high sun)	0.05 - 0.10
(low sun)	0.5 - 0.8
fresh snow	0.75 - 0.95
melting snow	0.35

6.3.1 Diffuse Irradiance Models for Tilted Surfaces

1. Liu and Jordan, 1963:

The diffuse sky radiance is assumed to be uniformly distributed (isotropic) over the sky dome. The diffuse radiation on a tilted surface is hence given by the horizontal diffuse radiation and the view factor from the surface to the sky $(1+\cos\beta)/2$:

$$G_{dt} = G_d \frac{(1+\cos\beta)}{2}, \tag{6.5}$$

where β is the slope of the plane.

Very simple, reasonably accurate

B.Y.H. Liu and R.C. Jordan (1963). The long-term average performance of flat-plate solar energy collectors. *Solar Energy*, **7**, 53ff.

Especially for cloudless skies, when the irradiance values (and thus the energy production of solar converters) are high, a more accurate modelling of the sky irradiance is needed, taking into account the anisotropy of the radiance distribution:

– preferential forward scattering *circumsolar radiation*
– increased scattering resulting from the longer pathlength near the horizon $\longrightarrow$ *horizon brightening*

Notes: For overcast sky conditions the isotropic assumption is appropriate.
In situations of partly cloudy skies the radiance distribution is more complex and strongly anisotropic.
$\longrightarrow$ Substantial variations of irradiance over sky hemisphere and with time!

2. Temps and Coulson, 1977:

Clear sky model considering horizon and circumsolar effects:

$$G_{dt} = G_d \frac{(1+\cos\beta)}{2} M_1 M_2, \tag{6.6}$$

with anisotropic modifiers reflecting the effect of circumsolar and horizontal brightening: $M_1 = 1+\sin^3(\beta/2)$, $M_2 = 1+\cos^2\theta \sin^3\theta_z$.

R.C. Temps and J.L. Coulson (1977). Solar radiation incident upon slopes of different orientations. *Solar Energy*, **19**, 179-184.

3. Klucher, 1979:

Introducing an additional cloudiness function F for all sky conditions:

$$G_{dt} = G_d \frac{(1+\cos\beta)}{2} M_3 M_4, \tag{6.7}$$

where $M_3 = 1 + F\sin^3(\beta/2)$, $M_4 = 1 + F\cos^2\theta\sin^3\theta_z$ and $F = 1 - (G_d/G)^2$.

For overcast skies $F = 0$ (isotropic distribution), for clear skies: $F = 1$ (same as the Temps and Coulson model)

T.M. Klucher (1979). Evaluation of models to predict insolation on tilted surfaces. *Solar Energy*, **23**, 111-1144.

4. Hay and Davies, 1980:

Approach: Overcast → no direct radiation → isotropic distribution
Absence of atmosphere → only direct radiation: $G_t = G(\cos\theta/\cos\theta_z)$

The actual state between these extremes is determined by the anisotropy index $\kappa = I_b/I_o$, giving the atmospheric transmissivity (diffuse radiation is divided into circumsolar and isotropically distributed diffuse radiation)

κ gives the portion of diffuse radiation to be treated as circumsolar and isotropic, respectively (no horizon brightening is considered);
G_{dt} is a linear combination based on the transmissivity for direct radiation.

$$G_{dt} = G_d \left\{ \kappa \frac{\cos\theta}{\cos\theta_z} + (1-\kappa)\frac{(1+\cos\beta)}{2} \right\} \tag{6.8}$$

J. Hay and J.A. Davies (1980). Calculation of the solar radiation incident on an inclined surface. Proc. First Canadian Solar Radiation Data Workshop (Ed. by J.E.Hay and T.K.Won). Canadian Atmospheric Environment Service, Downsview, Ontario. 59-72.

5. Perez et al., 1983:

Approach: Diffuse radiation is described by an isotropic background superimposed by two regions of enhanced radiation:

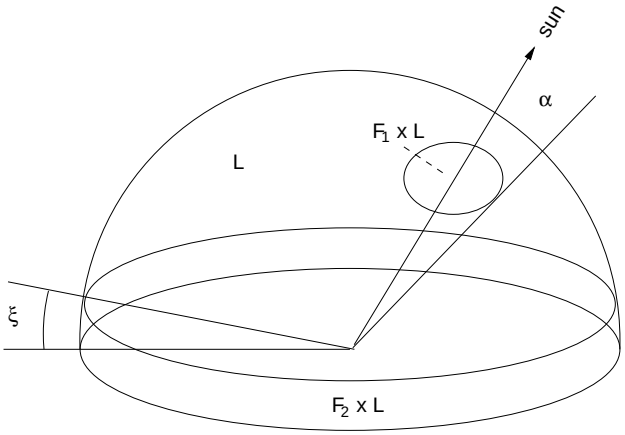

Fig. 6.2. Anisotropic components of diffuse sky radiation. Enhancements are due to circumsolar radiation and horizon brightening.

- a disk of variable size around the sun
- a horizontal band of variable height at the horizon.

The enhanced radiation is described by:
F_1: multiplier for circumsolar region (i.e. F_1 times the background (isotropic) radiation,
F_2: multiplier for horizon region.

$$G_{dt} = G_d \left\{ \frac{\left(\frac{1+\cos\beta}{2}\right) + a(F_1 - 1) + b(F_2 - 1)}{1 + c(F_1 - 1) + d(F_2 - 1)} \right\}, \tag{6.9}$$

where $a(\theta)$ and $b(\theta)$ are solid angles covered by the circumsolar disk and the horizon band, respectively multiplied by their average incidence on the considered plane (view factors to the receiver). $c(\theta_z)$ and d are the equivalent quantities for the horizontal (view factors to the horizontal).
F_1 and F_2 describe the sky condition and vary independently with the irradiance condition!
For isotropic distributions it is: $F_1 = F_2 = 0$.

Parameterized by:
- zenith angle θ_z,
- diffuse horizontal radiation G_d,
- $\epsilon = (G_{bn} + G_d)/G_d$.

$\rightarrow$ Large amount of categories (for each $[\theta_z, G_d, \epsilon]$ interval), i.e. 240 different pairs of F_1, F_2 parameters

R. Perez, J.T. Scott and R. Stewart (1983). An anisotropic model for diffuse radiation incident on slopes of different orientations, and possible applications to CPCs. Proceedings of ASES, Minneapolis, MN., 883-888.
R. Perez, R. Seals, P. Ineichen, R. Stewart and D. Menicucci (1987). A new simplified version of the Perez diffuse irradiance model for tilted surfaces. *Solar Energy*, **39**, 221-231.

6. Skartveit and Olseth, 1986:

A. Skartveit and J.A. Olseth (1986). Modelling slope irradiance at high latitudes *Solar Energy*, **36** 333-344.

6.3.2 Diffuse Fraction Models

Available solar radiation data primarily consists of global irradiation data on a horizontal surface. Since for many applications both the diffuse and the beam components are needed the problem arises of estimating the statistical relationship between the diffuse and the global component.

The fraction of the diffuse irradiation depends, at any moment, on geographical and astronomical factors (altitude of the site, zenith angle of the sun) and on climatological factors (turbidity, amount and type of clouds, surface albedo). Due to

the stochastic temporal variation of theses climatological quantities only statistical relationships can be obtained from the data. Assuming average atmospheric characteristics for a given site, which are assumed to depend only on the period of the year, a regressed relationship for the diffuse irradiation versus the global one can be derived.

The most common approach for decomposing the global radiation into their diffuse and global components is a model which relates the diffuse fraction to the clearness index:

$$\frac{G_d}{G} = f(k_t). \tag{6.10}$$

Typically, the empirical expressions for the diffuse fraction vary with the time interval under consideration (hourly, daily, monthly). For a given time period the relations are very similar despite being based on independent data.

Regressions of G_d/G vs k_t presented by Liu and Jordan in the 60s have been the main references for many years for deducing the daily and monthly diffuse irradiation from the corresponding global irradiation. Their analyses showed that these regressions are widely independent on location.

In recent years several investigations have been presented which showed a significant dependency on location and atmospheric condition.

Figure: Fraction of hourly diffuse radiation (G_d/G) as a function of the hourly clearness index k_t.

J.F. Orgill and K.G. Hollands (1977). Correlation equation for hourly diffuse radiation on a horizontal surface. *Solar Energy*, **19**, 357-359.

M. Collares-Pereira and A. Rabl (1979). The average distribution of solar radiation correlations between diffuse and hemispherical and between daily and hourly insolation values. *Solar Energy*, **22**, 155-164.

D.G. Erbs, S.A. Klein and J.A. Duffie (1982). Estimation of the diffuse radiation fraction for hourly, daily and monthly-average global radiation. *Solar Energy*, **28**, 293-304.

D.T. Reindl, W.A. Beckman and J.A. Duffie (1990). Diffuse fraction correlations. *Solar Energy*, **45** 1-7.

A. Skartveit and J.A. Olseth (1987). A model for the diffuse fraction of hourly global radiation *Solar Energy*, **38** 271-274.

Collares-Pereira and Rabl presented the following relations for daily data:

$$\frac{H_d}{H} = \begin{cases} 0.99 & \text{for } K_t \leq 0.17 \\ 1.188 - 2.272K_t + 9.473K_t^2 & \text{for } 0.17 < K_t \leq 0.75 \\ \quad -21.865K_t^3 + 14.648K_t^4 & \\ -0.54K_t + 0.632 & \text{for } 0.75 < K_t < 0.80 \\ 0.2 & \text{for } K_t \geq 0.80 \end{cases}$$

7. Statistical Properties of Solar Radiation

Optimal sizing procedures for solar energy systems (especially stand-alone (autonomous) systems) require accurate methods that take into account the stochastic nature of solar radiation and its sequential characteristics.

→ Time-series analysis of solar radiation data

– stationary properties: statistical moments

– frequency distribution (PDF)

→ use in analytical design procedures

– sequential properties: autocorrelation coefficient

⟶ Generation of synthetic radiation sequences

→ Numerical simulation and design

7.1 Statistical Variables

monthly mean clearness index
monthly variance of $X = K_t/\bar{K}_t$
monthly skewness of X

Problem: A month with average clearness index consists of days with varying K_t values related to the changing weather pattern. This influence can be described by the frequency of occurence of different K_t values.

Example: For a month with $\bar{K}_t$ = 0.5 the following daily pattern is observed:

4 days with $K_t < 0.2$	0.129 (cumulative frequency)
7 days with $K_t < 0.3$	0.225
10 days with $K_t < 0.4$	0.322
13 days with $K_t < 0.5$	0.419
19 days with $K_t < 0.6$	0.612
26 days with $K_t < 0.7$	0.838
31 days with $K_t < 0.8$	1.0

Empirical finding: months with same $\bar{K}_t$ show similar distribution of K_t (Liu and Jordan)

Continuous curve for the cumulative distribution $F(K_t)$ gives the frequency of occurence of days with $K_t' < K_t$.
From $F(K_t)$ the relative probability that the clearness index falls into a given range is:

$$P(K_{t,low} < K_t < K_{t,high}) = F(K_{t,high}) - F(K_{t,low}). \quad (7.1)$$

In the example data it is: P(0.3 $< K_t <$ 0.4) = 0.322 - 0.225 = 0.097, i.e., about 10 % of this month's days are in the K_t-range between 0.3 and 0.4.

Cumulative distribution function (CDF) → probability density function (PDF):

$$f(K_t) = \frac{dF(K_t)}{dK_t} \qquad \text{gradient of the cumulative distribution} \quad (7.2)$$

$$f(K_t) = \frac{P(K_t - \Delta K_t < K_t < K_t + \Delta K_t)}{\Delta K_t} \qquad \text{for } \Delta K_t < 0 \quad (7.3)$$

$$F(K_t) = \int_0^{K_t} f(K_t) dK_t \quad (7.4)$$

7.2 Generation of Synthetic Radiation Sequences

Obtaining hourly data on tilted planes:
1. generating synthetic daily K_t values from horizontal monthly $\bar{K}_t$ value
2. generating synthetic hourly k_t values from daily K_t values
3. calculating diffuse fraction for each hour
4. converting the diffuse and direct fractions for the horizontal to corresponding components for tilted surfaces

Method for synthetic hourly data is more complicated than for daily data due to the daily trend.

J. M. Gordon and T. A. Reddy (1988). Time series analysis of daily horizontal solar radiation. *Solar Energy*, **41**, 215-226.
R. Aguiar and M. Collares-Pereira (1992). TAG: A time-dependent, autoregressive, Gaussian model for generating synthetic hourly radiation. *Solar Energy*, **49**,167-174.

problem:
- extracting all relevant statistical information from measured solar radiation time series
- building a model based on these statistical parameters for a synthetic time series
- testing the model for generalized application model for synthetic daily radiation data (Gordon and Reddy):
- removing the trend from daily radiation data time series by using the clearness index K_t instead of the radiation H (extracting the influence of latitude)
- normalized statiastical variable: Especially, it is:
with variance
- The authors propose the empirical probability density function with
- generating the time series from the PDF requires knowledge of the sequential statistics: autoregressive method (AR model):
normal distributed daily averages of a random variable Z:
(1) is the autocorrelation coefficient for the delay of one day
- generally it is:

- is random noise with mean value and variance
- no autocorrelation: (1) = 0, high autocorrelation: (1) = 1
- method:
- choosing a random value for Z (normal distributed)
- calulating the cumulative function
where the + sign applies to $Z > 0$ and the - sign to $Z < 0$.
- using this value to calculate $X(d)$ from the empirical cumulative function
- calculate

8. Measurement of Solar Radiation

There are three major spectral regions in which measurements of solar radiation are desired: UV (UV-A, around 386 nm; UV-B, around 306 nm), Solar (0.3–3.0 μm, also known as VISIBLE radiation) and IR (greater than 3 μm).

There are different ways in which to measure the incoming (UV and solar) radiation. You can measure global, direct or diffuse radiation. Diffuse radiation measurement instruments cover the whole hemisphere (180 degrees viewing angle) and are shaded from the sun. The detector is placed horizontally. Direct radiation meters are aimed directly at the sun, so the detector surface is at right angles with the incoming radiation. When measuring global radiation, the instrument receives both the diffuse and direct component on a horizontally placed detector.

The requirements for measuring solar radiation are largely dependant on the accuracy that is wanted.

For measuring global solar radiation, the standard instrument is a pyranometer. Its equivalent for the far infrared range is called a pyrgeometer. For the UV range the instruments are UV, UV-A or UV-B radiometers.

By 'shading' a pyranometer from the direct radiation (coming directly from the sun) one can measure the diffuse radiation (coming from the hemisphere, not directly from the sun).

For the measurement of direct radiation one can either use a calculation (global minus diffuse, corrected for the cosine of the zenith angle of the sun) or a measurement with a tube shaped detector that has to be aimed at the sun. The latter instrument is called a pyrheliometer. A measurement with a pyrheliometer is more accurate, but at the same time it demands more attention. There exists also a pyrheliometer version of the UV radiometer.

All the instruments mentioned are available in different accuracy classes, varying from reference instruments (+/- 0.5 %) to second class instruments (roughly +/- 10 %).

Three of the basic instruments, pyranometer, pyrheliometer and pyrgeometer are all based on a thermal detector. This detector has a flat spectral response. The differences are in a filter material and in field of view. For a pyranometer and pyrheliometer the filter material, which also protects the sensor against environmental influences, is glass, only letting solar radiation (0.3–3 μm) pass. For a pyrgeometer, the material used is coated silicon, only allowing far infrared radiation (3–50 μm) to pass.

A pyrheliometer has a limited field of view (5 degrees opening angle). The thermal detectors have a small voltage output, linearly proportional to the incoming radiation. Since 1993, pyranometers and pyrheliometers have been characterized according to the ISO standard number 9060. This ISO standard can act as a guideline in choosing the right detector specification. There is no ISO standard defined for pyrgeometers or UV radiometers.

The UV radiometers are different in both detector type and filter specifications. UV-B and UV-A radiometers have a narrow band sensitivity. For the UV-B radiometer, the central wavelength is at 306 nm because the optimum effect is reached when the human skin (Erythermal) spectrum and the solar spectrum are multiplied. The UV-A radiometer central wavelength, 386 nm, is chosen because this particular wavelength is also used in the WMO air pollution network.

Ventilation of radiation meters improves the accuracy and the reliablity of the measurements. It minimizes certain offsets and keeps the measuring instruments free from dew and frost.

The second trend is combining the tracking of pyrheliometers and the shading of pyranometers.

8.1 Radiation Detectors

Radiation quantities which have to be measured in solar energy research and application:

- Total (global) irradiance Total amount of solar irradiance on an upward-facing surface; sum of vertical component of direct normal solar irradiance and the diffuse sky irradiance. It is measured either with a pyranometer or more accurately by summing the direct and diffuse horizontal irradiance.
- Diffuse irradiance
  Radiation that reaches the ground that has been scattered by the atmospheric constituents. It is measured with a pyranometer that is continually shaded from the direct solar irradiance.
- Direct irradiance
  Solar radiation passing directly through the atmosphere from the sun without being scattered or absorbed by the atmosphere. Typically it is measured on a surface that is kept normal to the direction the center of the suns disc by a solar tracker.
- Spectral irradiance
  higher spectral resolution than broadband measurements. Typically in spectral bands of several to a few 10s of nanometers. The direct irradiance in certain narrowband channels is measured by sunphotometers. These observations can be used to derive the total transmittance of the atmosphere within the respective spectral band which can in turn be used to deduce aerosol optical depths.
- Sunshine hours (sunshine duration)
  duration of sunshine, only qualitative

Only broadband instruments will be treated in detail!

Different types of radiometric detectors:

calorimetric: radiant energy absorbed by an high-conductivity metal (black painted) is converted into heat that is measured;
temperature rise is measure of irradiation → absolute instrument possible

thermomechanic: different thermal expansion properties of two metal stripes when exposed to radiation lead to different distortions, which are measured
example: pyranographs (inaccurate!)

thermoelectric: two junctions of dissimmilar metal wires at different temperature lead to a voltage difference (electromotive force), it is $V \sim \Delta T$ (Seebeck-effect). Examples: Copper-Constantan, Manganin-Constantan
thermopile sensors, usually: increasing EMF by coupling several thermocouples in series (thermopile)
important: cold junctions must be at constant temperature → thermal contact with massive brass plate
Plot: thermopile configurations

photoelectric: mainly photovoltaic effect, usually silicon solar cell detector, usually temperature compensated.
advantage: cheap, fast response; disadvantage: spectral sensitivity
frequently used in PV-plant monitoring!

Plot: PV-spectral sensitivity

8.2 Field Instruments

Mainly two different types of instruments are used referring to the radiation incident from the total hemisphere (solid angle 2π) or radiation coming only from the direction of the sun (direct normal radiation).

8.2.1 Global Radiation

Global radiation is the hemispherical solar radiation, i. e. the radiation received by a plane surface from the solid angle 2π steradian. Instruments measuring hemispherical solar radiation are called *pyranometer*.

Global radiation is measured by a pyranometer. Modern pyranometer using wirewound plated thermopiles, can be one of two types: With a black sensor protected by two precision ground, polished hemispheres or with a black and white ”star” sensor that is protected by a single polished hemisphere.

Over the years, there have been efforts to increase the linearity of response, durability, the adherence to the Lambert cosine response law and independence from ambient temperature effects.

Transformation of radiative energy to heat
→ temperature of the receiving surface is raised
→ steady state equilibrium is attained by heat losses to thermal sinks (instrument body, ambient air)
→ constant voltage

The main parts of a pyranometer are:
- thermal sensor (black painted surface)
- glass domes (protection, minimizing exchange of thermal radiation, IR-shield)
- instrument body

The required pyranometer accuracy can only be realized with detectors of the thermoelectric type. The temperature of the absorber is measured by a thermopile (series of thermocouples), whose active junctions are in contact with the absorber surface (Moll-Gorczynski-type). The passive junctions are connected to the instrument body, which therefore has to be shielded against the radiation. A remaining temperature dependence has to be compensated by an auxiliary thermistor circuitry.

differences in temperature by diff. paintings (black & white), diff. thermal insulation (CM 11), diff. radiation exposure (PSP)

sensor types: Eppley PSP, Kipp & Zonen CM 11, CM 21, Schenk

spectral sensitivity: nearly uniform in range 300–2800 nm (governed by glass dome absorption)

response time!

Plot: typical pyranometer data (K&Z data sheet)

Characteristics of Pyranometer. The values in parentheses give the specifications for first class pyranometer according to the WMO classification.

Response Time i.e. the time for reaching a certain percentage of the final measuring value due to the thermal inertia of the instrument (95 % value: < 30 sec)

Zero offset due to thermal radiation ($< 15\,\mathrm{Wm}^{-2}$ for $200\,\mathrm{Wm}^{-2}$ net thermal radiation, ventilated)

Non-stationarity caused by the ageing of the absorber surface ($< \pm 1$ % per year).

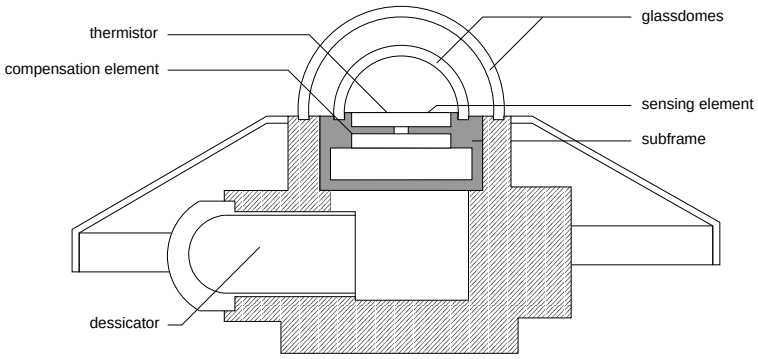

Fig. 8.1. Schematic construction of Kipp & Zonen CM 11 pyranometer.

Non-linearity The change in responsivity with irradiance level ($< \pm 1$ % from measured value at 500 Wm^{-2} over full range).

Cosine response The deviation in responsivity from the proportionality to the cosine of the angle of incidence ($\pm$ 2 % at 60 $^\circ$ angle of incidence, $\pm$ 5 % maximum deviation within 60 $^\circ$–80 $^\circ$.

Azimuth response The azimuthal variation of the deviation in responsivity from the cosine response ($\pm$ 5 % deviation from mean at 80 $^\circ$ angle of incidence).

Spectral selectivity governed by the glass dome and the absorber coating ($\pm$ 5 % maximum deviation in $\alpha\tau$ from average within the spectral range 0.35–1.5 μm).

Temperature response due to the changing ambient temperature (4 % deviation for a change of ambient temperature within an interval of 50 K).

Tilt response when the pyranometer is operated in an inclined position ($\pm$ 2 % deviation for vertical mounting and 1000 Wm^{-2}).

8.2.2 Direct Radiation

Direct radiation is measured by use of a pyrheliometer, which measures radiation at normal incidence. The pyrheliometer consists of a wirewound thermopile at the base of a tube, the aperture of which bears a ratio to its length of 1 to 10, subtending an angle of 543'30" (Eppley NIP). This limits the radiation that the thermopile receives to direct solar radiation only. The pyrheliometer is mounted on a solar tracker for continuous readings.

From small solid angle centered at the sun's disk
→ direct normal radiation
angular diameter of sun's disk: 0.5°.

instruments measuring direct solar irradiance are called *pyrheliometer*. Usually of thermoelectric type.

Components:
- thermal sensor (blackened surface, black cavity)
- (diaphragm) tube
- tracking device

typically full angle of view: 5–6°.

8.2.3 Diffuse Radiation

Diffuse radiation can either be derived from the direct radiation and the global radiation or measured by shading a pyranometer from the direct radiation so that the thermopile is only receiving the diffuse radiation.

The direct measurement of the diffuse radiation is performed by using a pyranometer which is shielded from direct solar radiation by a circular disk or a fixed shade ring (shadow band). A shading disk must be tracked to follow the suns path and therefore requires a huge amount of maintenance. Therefore operational stations are usually equipped with shade ring devices, which have to be adjusted to only follow the solar declination 1–2 times a week.

Because the shade ring covers parts of the diffuse sky instead of only the sun disk, a shading correction has to be applied. The correction factor depends on the pyranometer type, the geometry of the shade ring, the geographical latitude and the actual anisotropy of the sky radiance distribution. According to Drummond (1956) and Dehne (1984), isotropic and anisotropic correction factors are introduced through the empirical formulas, respectively:

$$f_{is} = \frac{1}{1 - KF}, \tag{8.1}$$

where $K = (b/r)\cos^3\delta$, $F = (2/\pi)(\omega_0 \sin\phi \sin\delta + \sin\omega_0 \cos\phi \cos\delta)$ and $\omega_0 = \arccos(-\tan\phi \tan\delta)$ is the sunset hour angle. b and r are the width and the radius of the shading ring, respectively. δ is the declination of the sun and ϕ the geographical latitude.

The anisotropic correction factor is expressed as a function of the uncorrected diffuse radiation $G_{d,uncorr}$, the global radiation G and the declination of the sun δ:

$$f_{an} = 1.064 - 0.067 \left(\frac{G_{d,uncorr}}{G} \right)^3 - 0.001\delta. \tag{8.2}$$

The corrected value of the diffuse radiation thus can be written:

$$G_{d,corr} = f_{is} f_{an} G_{d,uncorr}. \tag{8.3}$$

An indirect method of measuring the diffuse radiation is the simultaneous measurement of the global radiation G and the direct normal radiation $G_{b,n}$ using a pyranometer and a pyrheliometer. The diffuse radiation then is calculated using the relationship

$$G_d = G - G_{b,n} \cos\theta_z. \tag{8.4}$$

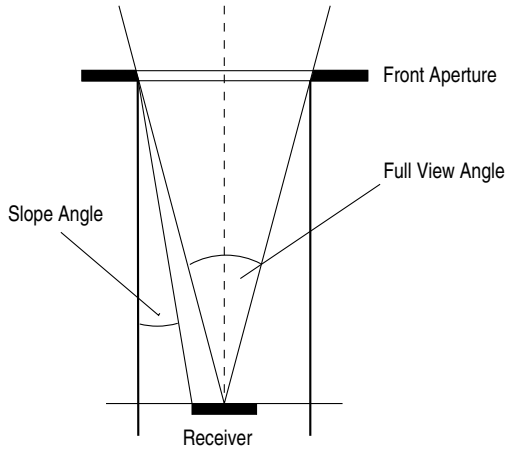

Fig. 8.2. View limiting geometry of a pyrheliometer.

8.3 Special Measurements

8.3.1 Ultraviolet Radiation

For the measurement of direct and diffuse ultraviolet radiation in the wavelength interval 0.295–0.385 μm, which is particularly important in environmental, biological, and pollution studies the Total Ultraviolet Radiometer (Model TUVR) can be used. This instrument utilizes a photoelectric cell protected by a quartz window. A specially designed teflon diffuser not only reduces the radiant flux to acceptable levels but also provides close adherence to the Lambert cosine law. An encapsulated narrow bandpass (interference) filter limits the spectral response of the photocell to the wavelength interval 0.295–0.385 μm.

8.3.2 Infrared Radiation

Net radiometers have been employed for longwave radiation beyond 3 μm for work in thermal balance but they were criticized for the fragile nature of their thin polyethylene domes and their requirement for compressors or nitrogen bottles for purging or ventilation. This problem is overcome by the Precision Infrared Radiometer (Eppley Model PIR).

8.3.3 Spectral Radiation

Spectral Radiometers are instruments like sunphotometers designed for observing certain narrow spectral bands of sunlight. They typically consist of interference glass filters and silicon detectors to measure solar radiation in a narrow spectral band (typically 5 nm FWHM). Mostly, filters are the source of considerable uncertainty and lack stability for long-term measurements. sunphotometers are used to determine the atmospheric turbidity (aerosol optical depth) and the concentration of trace gases such as ozone or water vapor. A sunphotometer is calibrated in terms of its extraterrestrial signal at 1 AU (astronomical unit) distance from the sun. When calibrated in absolute units, the sunphotometer can also be used to determine the solar spectral irradiance from stratospheric balloons, rockets or satellites.

8.3.4 Sunshine Duration

8.3.5 Atmospheric Turbidity

8.3.6 Surface Albedo

8.4 Radiation Standards

Self calibrating cavity pyrheliometers are used to define the scale of solar radiation. This type of instrument can be constructed and characterized to yield absolute radiation values in Standard International (SI) units by employing the electrical

substitution method. A selected group of these instruments is known as the World Standard Group (WSG) which is maintained at the World Radiation Center (WRC) in Davos, Switzerland. Using this group of instruments, the World Radiation Reference (WRR) is periodically determined. All other cavity instruments are referenced to the WRR by intercomparison.

The specification, the calibration and the use of pyranometers and pyrheliometers is covered by international standards. The most common standards are:

ISO 9060 : Specification and classification of instruments for measuring hemispherical solar and direct solar radiation. This standard covers the specification, and can serve as a guide when selecting instruments for a particular application.

ISO TR 9901 : Field pyranometers, recommended practice for use. This standard covers selection, installation and maintenance of pyranometers.

ISO 9847 : Calibration of field pyranometers by comparison to a reference pyranometer. This standard covers calibration, both during use in the field and indoors.

8.5 Operation, Maintenance and Calibration of Instruments

9. Estimating Surface Irradiance from Satellite Data

9.1 The HELIOSAT Method

The general idea of the HELIOSAT method for the estimation of surface solar irradiance from satellite images is to deal with atmospheric and cloud extinction separately. In a first step the clear sky irradiance for a given location and time is calculated. In a second step a cloud index is derived from METEOSAT imagery to take into account the cloud extinction. This step uses the fact that the reflected radiance measured by the satellite is approximately proportional to the amount of cloudiness characterized by the cloud index. This value then is correlated to the cloud transmission. Finally, the clear sky irradiance is reduced due to the cloud transmission to infer the surface irradiance. Figure 9.1 gives an overview of the algorithms to calculate the surface irradiance from a satellite image. The top and lefthand side corresponds to the first step and the righthand side to the second step.

Details of the algorithm as well as the derivation of additional quantities used in solar energy applications are described in the following sections.

9.1.1 Clear Sky Irradiance

The HELIOSAT method was originally proposed by Cano and later modified by Beyer et al. and Hammer. For the calculation of the clear sky irradiance a direct irradiance model of Page and a diffuse irradiance model of Dumortier are used. These models were developed by an empirical analysis of ground data. Both use the Linke turbidity factor to describe the atmospheric extinction. The direct normal irradiance G_{dn} is then given by:

$$G_{dn,clear} = G_{sc} \cdot \epsilon \cdot e^{-0.8662 \cdot T_L(2) \cdot \delta_R(m) \cdot m} \tag{9.1}$$

where G_{sc} is the solar constant, ϵ the eccentricity correction, $T_L(2)$ the Linke turbidiy factor for air mass 2, $\delta_R(m)$ the Rayleigh optical thickness and m the air mass.

The eccentricity correction ϵ is given by:

$$\epsilon = 1.000110 + 0.034221 \cos \Gamma + 0.001280 \sin \Gamma + 0.000719 \cos 2\Gamma + 0.000077 \sin 2\Gamma$$

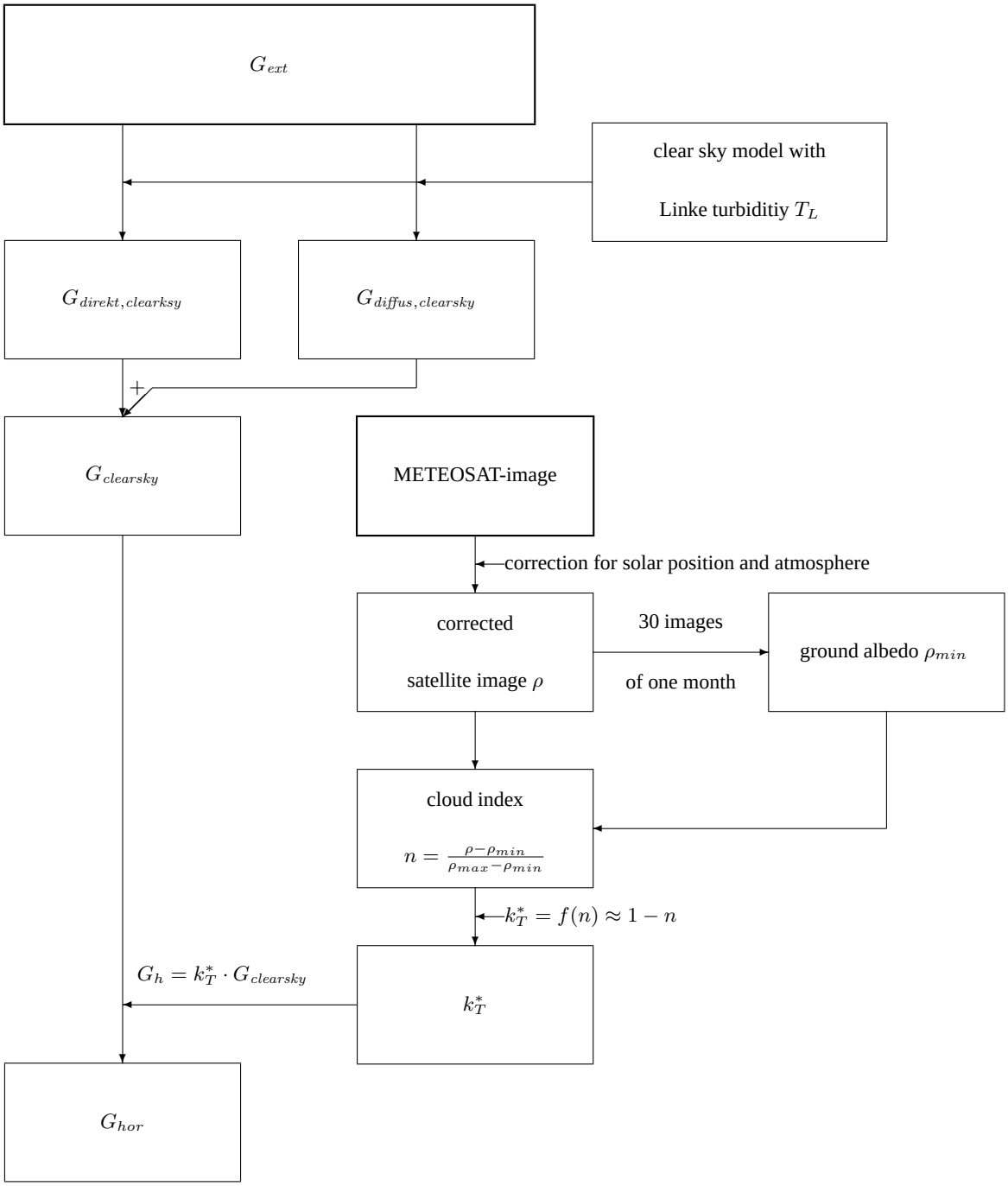

Fig. 9.1. Overview of the HELIOSAT method

(9.2)

with

$$\Gamma = 2\pi \frac{J-1}{365}. \tag{9.3}$$

Here, J corresponds to the day of year.
Air mass is calculated using an expression introduced by Kasten and Young:

$$m = \frac{1 - z/10000}{cos\theta_z + 0.50572(96.07995 - \theta_z)^{-1.6364}}, \tag{9.4}$$

with the height z of the site in meters and the zenith angle θ_z of the sun in degrees. The Rayleigh optical thickness $\delta_R(m)$ is the optical thickness of a dry and clean atmosphere, where only Rayleigh scattering occurs. According to Kasten and Page for $m < 20$ it can be approximated by:

$$\delta_R = \frac{1}{6.6296 + 1.7513m - 0.1202m^2 + 0.0065m^3 - 0.00013m^4} \tag{9.5}$$

and for $m > 20$ by:

$$\delta_R = \frac{1}{10.4 + 0.718m}. \tag{9.6}$$

The Linke turbidity is defined as the number of Rayleigh atmospheres necessary to represent the actual optical thickness $\delta(m)$:

$$T_L = \frac{\delta(m)}{\delta_R(m)} \tag{9.7}$$

Since the turbidity still shows a daily variation, it is normalized to the turbidity for air mass 2:

$$T_L(2) = \frac{T_L(m) \cdot \delta_R(m)}{\delta_R(2)}. \tag{9.8}$$

The diffuse irradiance is calculated using an empirical relationship by Dumortier:

$$\begin{aligned} G_{dif} = G_{ext} \cdot \epsilon \cdot (&0.0065 + (-0.045 + 0.0646 \cdot T_L(2)) \cdot cos\theta_z \\ &+ (0.014 - 0.0327 \cdot T_L(2)) \cdot cos^2\theta_z). \end{aligned} \tag{9.9}$$

G_{ext} is the extraterrestrial irradiance on a horizontal plane.

Since the spectral channels of METEOSAT do not supply any information on atmospheric turbidity a climatological model is applied. To account for the annual variation of the turbidity a relation of Bourges is used:

$$T_L(2) = T_0 + u \cos\left(\frac{2\pi}{365} J\right) + v \sin\left(\frac{2\pi}{365} J\right), \tag{9.10}$$

T_0, u and v are site specific parameters, A map specifying the parameters for Europe has been set up during the EU-funded *Satel-Light* project (www.satel-light.com).

Finally the total clear sky irradiance is the sum of the components:

$$G_{clear} = G_{dn,clear} \cdot \cos\theta_z + G_{dif,clear} \tag{9.11}$$

9.1.2 Cloud Transmission

Clouds have the largest influence on atmospheric radiative transfer. The cloud amount is derived from METEOSAT imagery. First the METEOSAT images are normalized with respect to the solar zenith angle. Therefore a relative reflectance ρ is introduced:

$$\rho = \frac{C - C_0}{G_{ext}}. \tag{9.12}$$

Here C is the measured pixel intensity of the satellite radiometer and C_0 is a total offset resulting from an instrument offset C_{off} and an atmospheric offset C_{atm} due to atmospheric backscattering. An empirical relationship for C_{atm} was derived from an analysis of ocean pixels:

$$C_{atm} = \left(1 + \cos^2\Psi\right) \cdot \frac{f(\theta_z)}{cos^{0.78}\phi}, \tag{9.13}$$

where Ψ is the angle between sun and satellite as seen from the ground and ϕ the zenith angle of the satellite. Ocean pixels are used because the surface reflectance of oceans in the direction of the satellite can be neglected. The measured reflectance therefore nearly completely results from the atmosphere. The function $f(\theta_z)$ is:

$$f(\theta_z) = -0.55 - 25.2 \cdot \cos\theta_z - 38.3 \cdot \cos^2\theta_z + 17.7 \cdot \cos^3\theta_z. \tag{9.14}$$

The total offset C_0 then is

$$C_0 = C_{off} + C_{atm}. \tag{9.15}$$

The measured reflectance is usually low for earth surfaces and high for clouds. Therefore a cloud index n as a measure of the cloud cover is introduced. It varies between 0 for cloud free and 1 for overcast conditions and uses the relative reflectivity ρ from equation (9.12):

$$n = \frac{\rho - \rho_{min}}{\rho_{max} - \rho_{min}}. \tag{9.16}$$

ρ_{min} corresponds to the surface albedo. Maps of the surface albedo are computed on a monthly basis by a statistical analysis of the dark pixels. The monthly calculation is done to account for seasonal variations of the ground reflectance. The maximum reflectivity ρ_{max} is computed separately for each satellite radiometer due to differences in the sensor properties in the different METEOSAT satellites.

Cloud transmission can be described by the clearsky index k_T^* which normalizes the actual surface irradiance G with the clear sky irradiance G_{clear} from equation (9.11):

$$k_T^* = \frac{G}{G_{clear}}. \tag{9.17}$$

The clear sky index k_T^* is calculated using a simple relationship with the cloud index n. The relationship is shown in figure 9.2. It has been derived within the *Satel-Light* project:

$$\begin{aligned} n \leq -0.2 \qquad & k_T^* = 1.2 \\ -0.2 < n \leq 0.8 \qquad & k_T^* = 1 - n \\ 0.8 < n \leq 1.1 \qquad & k_T^* = 2.0667 - 3.6667 \cdot n + 1.6667 \cdot n^2 \\ 1.1 < n \qquad & k_T^* = 0.05 \end{aligned} \tag{9.18}$$

Fig. 9.2. Relation between cloud index n and clear sky index k_T^* used in the HELIOSAT method.

Equations (9.11) and (9.17) are then used to obtain the surface irradiance G:

$$G = k_T^* \cdot (G_{dn,clear} \cdot \cos\theta_z + G_{dif,clear}) \tag{9.19}$$

The direct and diffuse irradiance are taken from equations (9.1) and (9.9), respectively.

9.1.3 Direct and Diffuse Irradiance

For most solar energy applications the irradiance in the plane of the solar converter is of interest rather than the global horizontal irradiance. For example, daylight applications often need data for vertically oriented planes. In these cases the fractions of direct and diffuse irradiance also have to be known to convert the horizontal irradiances to the tilted planes.

The direct and diffuse component of the surface irradiance is derived using a statistical model of Skartveit and Olseth based on hourly values of the global irradiance. It uses the clearness index k_T, the solar zenith angle and an hourly variability index σ_3 for the calculation of the diffuse fraction. The clearness index k_T is the global irradiance normalized with the extraterrestrial irradiance G_{ext}:

$$k_T = \frac{G}{G_{ext}}. \tag{9.20}$$

The hourly variability index σ_3 is determined from the clearness indices of three consecutive hours. If k_{T_i} is the clearness index of the hour i, then σ_3 is defined as:

$$\sigma_3 = \sqrt{\frac{(k_{T_i} - k_{T_{i-1}})^2 + (k_{T_i} - k_{T_{i+2}})^2}{2}}. \tag{9.21}$$

Figures 9.3 and 9.4 show the diffuse fraction for two solar elevations. The expected decrease of the diffuse fraction with increasing clearness index reverses for large clearness index values. This is due to additional reflections by clouds especially under broken cloud conditions. The diffuse fraction is generally higher for large solar zenith angles, because of increased scattering due to the longer path length.

Fig. 9.3. Diffuse fraction d versus clearness index k_T and variability index σ_3 = 0.0, 0.1 and 0.3 for a solar zenith angle of 80°.

Fig. 9.4. Diffuse fraction d versus clearness index k_T, variability index σ_3 = 0.0, 0.1 and 0.3 for a solar zenith angle of 40 °.

9.1.4 Illuminance

Illuminance is the radiant flux density from visible radiation. Illuminances are are gained by weighting the global irradiance with the spectral spectral sensitivity of

the human eye. They form the most appropriate inputs for the analysis of daylight applications i.e. the analysis and optimization of architectural concepts to minimize the need of artificial lighting in buildings. Illuminances are calculated from the irradiances using the luminous efficacy model from Olseth. The luminous efficacy describes the conversion of irradiance to illuminance. The model is based on the CIE (International Commission on Illumination) curve for photopic vision and on spectral irradiances obtained by an interpolation between transmittance models for cloudless skies and unbroken cloud cover. The model has been parameterized and requires solar elevation, the day of year and diffuse and direct normal clearness indices as input.

Fig. 9.5. Meteosat image, 1 October 2002, 12 UTC.

Fig. 9.6. Ground albedo, 1 October 2002, 12 UTC.

Fig. 9.7. Irradiance map, 1 October 2002, 12 UTC.

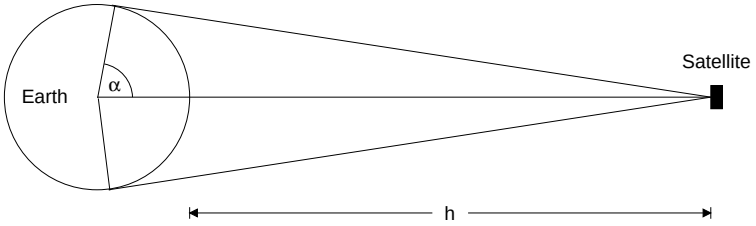

Fig. 9.8. Earth-satellite system. The height h of the geostationary METEOSAT satellite is 35800 km. The view angle α is 81°.

10. Solar Radiation Data

10.1 .....

10.2 ....

Part II

Wind Energy

11. Introduction

11.1 Wind Energy Conversion Paths

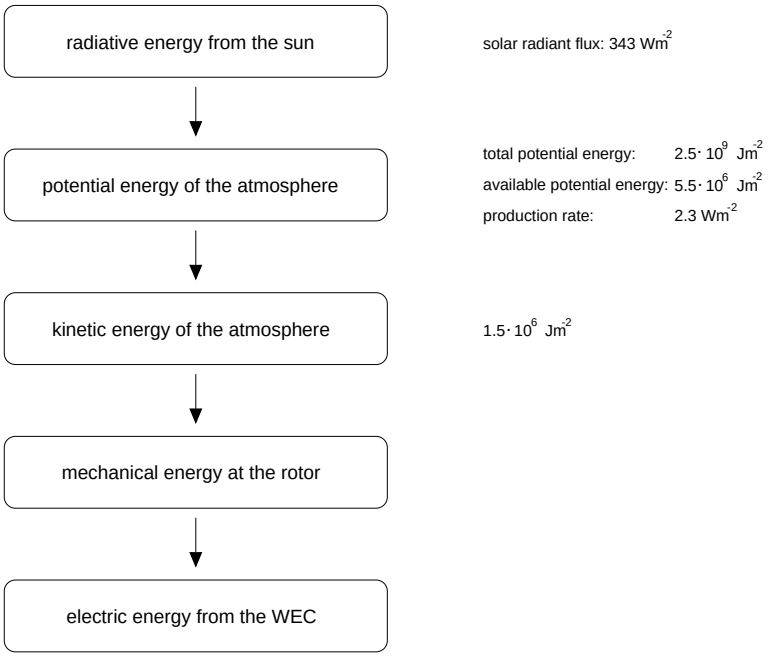

Fig. 11.1. Wind energy conversion flow diagram from irradiated solar energy to electric energy produced by a wind turbine. The values given for the energies and energy fluxes are long term global averages.

12. Origin of Atmospheric Motions

12.1 Available Potential Energy

The total energy of the atmosphere can be devided into the

- internal energy
- gravitational potential energy
- kinetic energy.

Internal and gravitational potential energy are often summarized as total potential energy.

Internal energy E_i of a unit column of air:

$$E_i = c_v \int_0^\infty \rho T dz, \tag{12.1}$$

where c_v = 717 Jkg^{-1}K^{-1} is the specific heat of dry air at constant volume, ρ is the air density and T is the temperature. Generally, it is: $E_i = mc_vT$ with mass m.

Gravitational potential energy E_p of a unit column of air:

$$E_p = \int_0^\infty \rho g z dz = -\int_{p_0}^0 z dp = R \int_0^\infty \rho T dz, \tag{12.2}$$

where R = 287 Jkg^{-1}K^{-1} is the gas constant for dry air, g is the acceleration due to gravity, z is the height above ground and p_0 is the air pressure at the bottom of the column. Generally, it is: $E_i = mgh$.

With the specific heat at constant pressure c_p = 1004 Jkg^{-1}K^{-1} the total potential energy of the atmosphere (sum of internal and gravitational potential energy) can be written:

$$E_p + E_i = \frac{c_p}{R} E_p = \frac{c_p}{c_v} E_i. \tag{12.3}$$

Only a very small fraction of the total potential energy of the atmosphere is available for conversion to kinetic energy. The kinetic energy E_k of a unit column of air is:

$$E_k = \frac{1}{2} \int_0^\infty \rho v^2 dz. \tag{12.4}$$

The generation of available potential energy and kinetic energy in the atmosphere is demonstrated by the simple model atmosphere shown in Fig. 12.1. Two air masses at a different temperature are seperated by a wall. Across the wall horizontal gradients of p, ρ, T have been established.

Removing the wall leads to:

– rearrangement of the air masses
– stable hydrostatic balance
– warm air completely above cold air mass.

The difference between the total potential energy at start- and at end-point of the rearrangement is called the *available potential energy*.

High horizontal pressure gradient $\longrightarrow$ high available potential energy

12.2 Heat Balance of the Atmosphere

The radiation budget at the top of the atmosphere for the whole earth is balanced in the long time average. That is, the incoming short wave radiation equals the outgoing longwave radiation leading to a stable temperature regime for the earth-atmosphere system.

The differential heating of the earth results in an availability of parts of the total potential energy of the atmosphere for conversion into kinetic energy. An atmosphere which is in an hydrostatic equilibrium (i.e.: no horizontal gradients of p, ρ, T) has no kinetic energy. It is in rest!

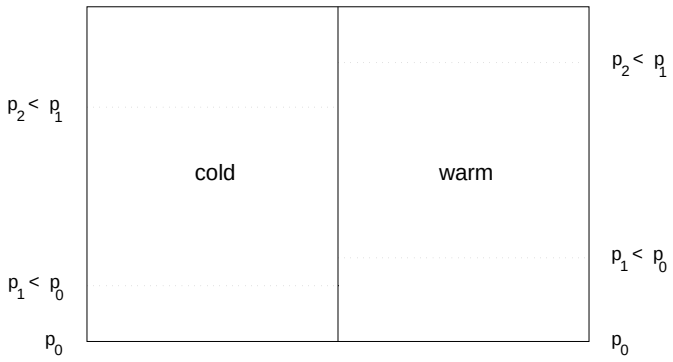

Fig. 12.1. Air columns of different temperatures resulting in a horizontal pressure gradient.

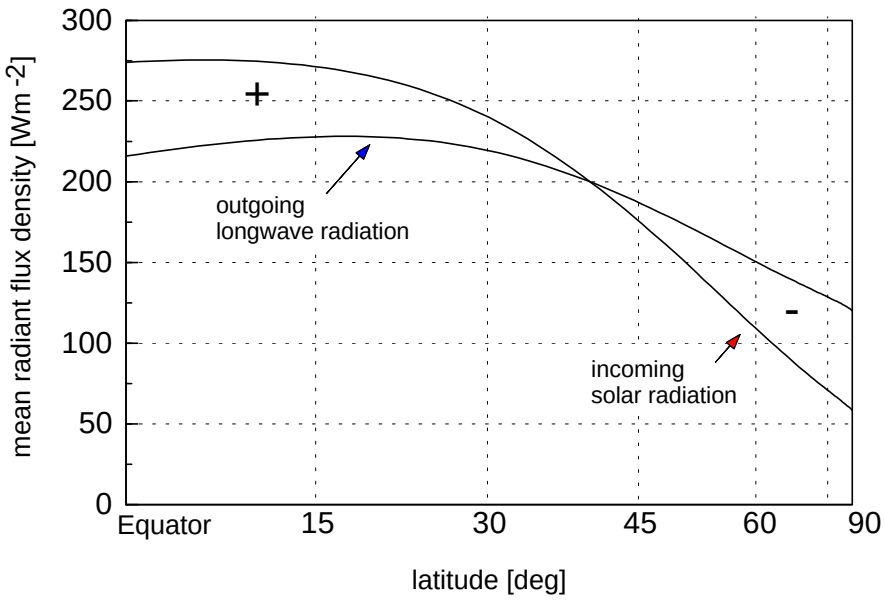

Fig. 12.2. Annual zonal mean estimates of absorbed solar radiation and outgoing longwave flux.

13. Physical Principles of Atmospheric Motion

The flow of air in the atmosphere is basically described by Newton's second law known from classical mechanics, which describes the relationship between forces acting on an object and the acceleration they cause in an inertial reference system. In vector notation, the general form is:

$$\boldsymbol{F} = m\boldsymbol{a}, \tag{13.1}$$

where m is the object's mass. The actual form of the equation depends on the forces that dominate the given flow. These forces will be discussed in the following subsections.

13.1 Forces Acting on an Air Parcel

13.1.1 Static State

pressure force $p = F/A$ (force/area)
units: Nm^{-2} = $\mathrm{kgs}^{-2}\mathrm{m}^{-1}$ = Pa (Pascal)
In meteorology commonly the unit 1 hPa = 100 Pa = 1 mbar is used.

Assuming air in rest: The pressure force is a measure of the weight of an air column above a unit area (static pressure).
Note: This reflects two different physical concepts: Pressure acts in all directions (scalar), the pressure force (vector) acts in one direction only.

The weight G of a column of air with height h and base area A is:

$$G = mg = \rho g V = \rho g A h, \tag{13.2}$$

where V is the volume of the column.

The pressure then is:

$$p = \frac{F}{A} = \frac{G}{A} = g\rho h. \tag{13.3}$$

This is the hydrostatic pressure, which is only exact in the abscence of vertical air motions.

Assuming a thin layer of the column, Eq. 13.3 results in

$$dp = -g\rho\, dz \tag{13.4}$$

and the surface pressure

$$p_0 = \int_0^\infty g\rho\, dz. \tag{13.5}$$

Eq. 13.4 is the *hydrostatic equation*, which describes the hydrostatic equilibrium between the gravitational force and the pressure gradient force.

13.1.2 Differences in Air Pressure

resulting in an additional force: pressure gradient force

With $F = pA$ it is (Fig. 13.1):

$$F_{x,l} = p\delta y\delta z \tag{13.6}$$

$$F_{x,r} = -(p + \frac{\partial p}{\partial x}\delta x)\delta y\delta z \tag{13.7}$$

$$F_x = -\frac{\partial p}{\partial x}\delta x\delta y\delta z \tag{13.8}$$

$$= -\frac{\partial p}{\partial x}\delta V \tag{13.9}$$

$$= -\frac{m}{\rho}\frac{\partial p}{\partial x} \tag{13.10}$$

Analogue for components in y and z directions:

$$F_y = -\frac{m}{\rho}\frac{\partial p}{\partial y}; \qquad F_z = -\frac{m}{\rho}\frac{\partial p}{\partial z} \tag{13.11}$$

Vector addition:

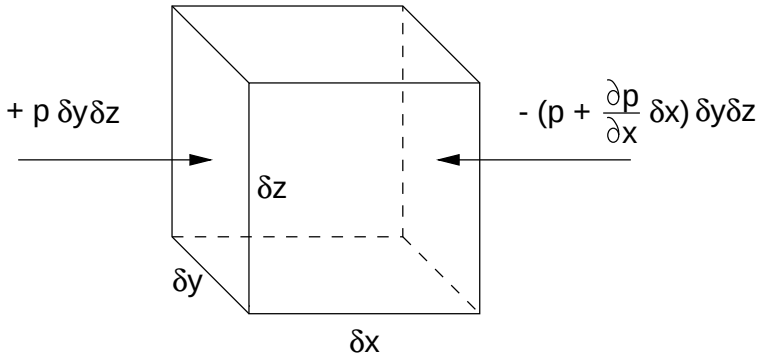

Fig. 13.1. The x-component of the pressure gradient force acting on a fluid element.

$$\boldsymbol{F} = -\frac{m}{\rho}\boldsymbol{\nabla} p \tag{13.12}$$

with gradient of p

$$\boldsymbol{\nabla} p = (\frac{\partial p}{\partial x}, \frac{\partial p}{\partial y}, \frac{\partial p}{\partial z}). \tag{13.13}$$

$\boldsymbol{\nabla}$ is an operator producing the vector gradient of a scalar field. $\boldsymbol{\nabla} p$ is a vector normal to the isobars (lines with p = const.).

The horizontal component of the pressure gradient force is:

$$\boldsymbol{F}_h = -\frac{m}{\rho}\boldsymbol{\nabla}_{\boldsymbol{h}} p. \tag{13.14}$$

Horizontal gradients in pressure cause pressure gradient forces perpendicular to the pressure isolines (isobars, lines with p = const.) directed from low to high pressure:

$$\boldsymbol{F}_p \sim \boldsymbol{\nabla} p. \tag{13.15}$$

14. Fundamental Forces

14.1 Forces for Vertical Air Motions

Acting forces:
- vertical pressure gradient force per unit mass: $\boldsymbol{a}_{p,v} = -1/\rho \, \partial p/\partial z$
- gravitational force: $\boldsymbol{a}_g = g$

Equation of motion:

$$\underbrace{\frac{dv_v}{dt}}_{10^{-7}\ ms^{-2}} = -\underbrace{\frac{1}{\rho}\frac{\partial p}{\partial z}}_{10\ ms^{-2}} - \underbrace{g}_{10\ ms^{-2}} \tag{14.1}$$

If typical magnitudes for the accelerations given in Eq. (14.1) are assessed, it is shown that in most cases in good approximation the vertical acceleration can be neclected compared to the driving forces in the vertical direction. Thus, the vertical pressure gradient force and the gravitational force are balanced (in large scale). This state is called the *hydrostatic equilibrium*:

$$-\frac{1}{\rho}\frac{\partial p}{\partial z} - g = 0 \tag{14.2}$$

or

$$\frac{\partial p}{\partial z} = -g\rho, \tag{14.3}$$

where g = 9.81 ms^{-2} is the gravitational acceleration at sea level.

For an atmosphere in a hydrostatic balance the decrease in pressure near the ground ($\rho = \rho_0$) can be calculated from Eq. (14.3):

$$\partial p/\partial z = -1.225\ \text{kg m}^{-3} \cdot 9.81\ \text{ms}^{-2} = -0.12\ \text{hPa/m} \tag{14.4}$$

and

$$\partial z/\partial p = -8.3\ \text{m/hPa}. \tag{14.5}$$

14.2 Forces for Horizontal Air Motion

Fluid elements are influenced by
– horizontal pressure gradient force
– Coriolis force
– friction (viscous) force

14.2.1 Horizontal Pressure Gradient Force

From spatial pressure differences given by the horizontal pressure gradient $\boldsymbol{\nabla_h} p$ it follows:

$$\boldsymbol{F}_{h,p} = -\frac{m}{\rho}\boldsymbol{\nabla_h} p \tag{14.6}$$

and

$$\boldsymbol{a}_{h,p} = -\frac{1}{\rho}\boldsymbol{\nabla_h} p. \tag{14.7}$$

$\boldsymbol{F}_{h,p}$ and $\boldsymbol{a}_{h,p}$ are directed perpendicular to the isobars towards low pressure.

14.2.2 Coriolis force

Particle movements on the earth can be separated into two parts:
– movement with respect to the earth surface
– rotation with the earth.

In a rotating coordinate system (fixed to the earth's surface) an additional virtual [1] force has to be considered, the *Coriolis force*. It acts only on moving particles. (This is different from the centrifugal force, an other virtual force that acts even on particles in rest with respect to the earth surface.)

Qualitative description
Example: Meridional movement of a particle in North-South direction.
The rotational speed of a particle depends on latitude and decreases from its maximum value at the equator (1670 km/h) to 0 km/h at the poles.

For particles moving from the equator towards North the principle of conservation of angular momentum causes a higher rotational speed as that of their environment. For an observer on the earth surface (i.e. on the rotational reference system) this is an virtual deflection of the particle to the right.
(Note: This is valid for motions in the northern hemisphere. In the southern hemisphere the deflection is to the left.)

Example: Zonal movements in East-West direction.
Motions in zonal directions lead to changes in the centrifugal force $\Omega^2 R$: eastward: increasing , westward: decreasing.

[1] This force is of a virtual nature because of its abscence in an absolute space-fixed coordinate system.

Motions from West to East cause an acceleration towards the equator and vertically upward (East to West vice versa). This again is a virtual deflection to the right (in the northern hemisphere).

Mathematical description:

A formal description of the apparent forces acting on moving objects in a rotating system can be derived by a transformation of coordinates between the inertial reference frame and the reference frame rotating with the angular velocity of the earth. The motion of an object with respect to a rotating system can be described by the relationship between the total derivatives [2] of a position vector in an inertial reference frame and in the rotating system:

$$\frac{d'\boldsymbol{r}}{dt} = \frac{d\boldsymbol{r}}{dt} - [\boldsymbol{r} \times \boldsymbol{\Omega}], \tag{14.8}$$

where $d'\boldsymbol{r}/dt$ and $d\boldsymbol{r}/dt$ are the respective rates of change of $\boldsymbol{r}$ in the inertial and the rotating system and the second term on the right-hand side is the contribution due to the rotation of the system with the angular velocity Ω. Applying Eq. (14.8) to the velocity vector $\boldsymbol{v} = d'\boldsymbol{r}/dt$ gives

$$\frac{d'}{dt}\frac{d'\boldsymbol{r}}{dt} = \frac{d}{dt}\frac{d'\boldsymbol{r}}{dt} - \left[\frac{d'\boldsymbol{r}}{dt} \times \boldsymbol{\Omega}\right] \tag{14.9}$$

[2] The total derivative is the rate of change of a given quantity following the motion.

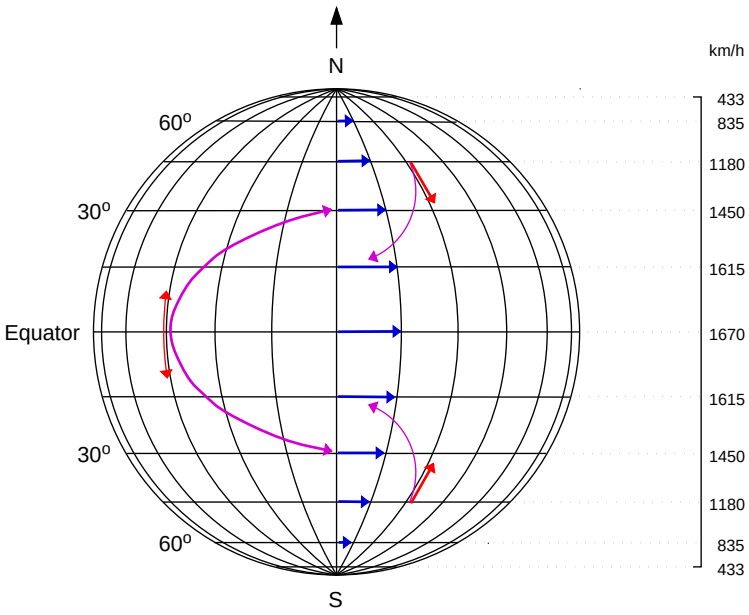

Fig. 14.1. The Coriolis force acting on particles which move meridionally. The right scale gives the rotational speed of the earth surface for a given latitude.

and after substituting (14.8) into (14.9)

$$\frac{d^{2'}\boldsymbol{r}}{dt^2} = \frac{d}{dt}\left(\frac{d\boldsymbol{r}}{dt} - \left[\boldsymbol{r}\times\boldsymbol{\Omega}\right]\right) - \left[\left(\frac{d\boldsymbol{r}}{dt} - \left[\boldsymbol{r}\times\boldsymbol{\Omega}\right]\right)\times\boldsymbol{\Omega}\right] \tag{14.10}$$

$$= \frac{d^2\boldsymbol{r}}{dt^2} - 2\left[\frac{d\boldsymbol{r}}{dt}\times\boldsymbol{\Omega}\right] + \left[\left[\boldsymbol{r}\times\boldsymbol{\Omega}\right]\times\Omega\right]. \tag{14.11}$$

Eq. (14.11) states that the acceleration in an inertial system equals the acceleration relative to the rotating system plus the Coriolis acceleration (second term) plus the centripetal acceleration (third term).

Vector notation of the Coriolis force and acceleration, respectively:

$$\boldsymbol{F}_c = -2m[\boldsymbol{\Omega}\times\boldsymbol{v}] \tag{14.12}$$

$$\boldsymbol{a}_c = -2[\boldsymbol{\Omega}\times\boldsymbol{v}] \tag{14.13}$$

where $\boldsymbol{\Omega} = (0, \Omega\cos\phi, \Omega\sin\phi)$ is the vector of the earth's rotation ($|\Omega| = 7.29\cdot 10^{-5}$ rad s^{-1}).

In its cartesian components, the Coriolis acceleration is:

$$\begin{aligned}\boldsymbol{a}_c = {} & 2(\Omega v\sin\phi - 2\Omega w\cos\phi)\,\boldsymbol{i}\\ & - 2\Omega u\sin\phi\,\boldsymbol{j}\\ & + 2\Omega u\cos\phi\,\boldsymbol{k},\end{aligned}$$

Usually, the vertical component of the Coriolis force is small compared to the gravitational force and vertical wind speeds are much smaller than horizontal ones, so that these terms can be neglected leaving only horizontal components:

$$\begin{aligned}\boldsymbol{a}_c \approx \boldsymbol{a}_{c,h} &= -2\Omega\sin\phi[\boldsymbol{k}\times\boldsymbol{v}_h]\\ &= -f[\boldsymbol{k}\times\boldsymbol{v}_h],\end{aligned} \tag{14.14}$$

where $f = 2\Omega\sin\phi$ ($\sim 10^{-4}\ s^{-1}$ in midlatitudes) is the *Coriolis parameter*. From Eq. 14.14 it is clear, that the Coriolis force vanishes at the equator and is perpendicular to the horizontal wind vector $\boldsymbol{v}_h$.

14.2.3 Friction Force

The air motion is slowed down at the earth's surface due to the friction force acting in the lowest layers of the atmosphere ($z < \sim 1000\ m$). For $z = 0$, it is $\boldsymbol{v}_h = 0$. The friction force is determined by

- wind velocity
- surface roughness
- thermal stability of the atmosphere.

A simple relationship for the friction force is:

$$\boldsymbol{F}_{fr,h} = -m\mu\boldsymbol{v}_h; \qquad \boldsymbol{a}_{fr,h} = -\mu\boldsymbol{v}_h \tag{14.15}$$

with the friction (or viscous) coefficient μ.
The friction force is directed opposed to the wind flow.

The friction force is mentioned here only to complete the list of forces acting on an air parcel. Its detailed description is out of the scope of this text, but is of major importance for the description of turbulent flows in the atmospheric boundary layer.

14.3 Equation of Motion

Horizontal motions of fluid elements in the atmosphere are governed by the acting forces introduced in section 14.2:

$$\boldsymbol{F}_h = \boldsymbol{F}_{p,h} + \boldsymbol{F}_{c,h} + \boldsymbol{F}_{fr,h}. \tag{14.16}$$

The individual acceleration of fluid elements (air parcels) thus is:

$$\frac{d\boldsymbol{v}_h}{dt} = \boldsymbol{a}_h = \boldsymbol{a}_{p,h} + \boldsymbol{a}_{c,h} + \boldsymbol{a}_{fr,h}. \tag{14.17}$$

Inserting from Eq. (14.7), (14.14) and (14.15), the *horizontal equation of motion* can be written:

$$\frac{d\boldsymbol{v}_h}{dt} = -\frac{1}{\rho}\boldsymbol{\nabla_h} p - f(\boldsymbol{k} \times \boldsymbol{v}_h) - \mu \boldsymbol{v}_h \tag{14.18}$$

Note: Accelaration is due to a change in velocity of the motion as well as due to a change in direction of the motion.

14.4 Balances of the Horizontal Wind Field

14.4.1 Geostrophic Balance

Assuming a parcel of fluid in a height above the surface, where it does not experience any influence of the underlying surface on its flow, i.e., no friction force is acting on it. Comparing the typical magnitudes of the acceleration term and of the acting forces:

- acceleration: 10^{-4} ms^{-1},
- forces: 10^{-3} ms^{-1}

In good approximation, the acceleration can be neglected in most situations and an equilibrium between the horizontal pressure gradient force and the Coriolis force is established:

$$-\frac{1}{\rho}\boldsymbol{\nabla_h} p = f(\boldsymbol{k} \times \boldsymbol{v}_h) \tag{14.19}$$

or

$$\boldsymbol{v}_h = -\frac{1}{\rho f}\boldsymbol{\nabla_h} p \times \boldsymbol{k}. \tag{14.20}$$

The wind speed $\boldsymbol{v}_h$ representing this balance is called the *geostrophic wind* v_g and is written in absolute terms as

$$v_g = -\frac{1}{\rho f}\nabla_h p. \tag{14.21}$$

Fig. 14.2 shows that $\boldsymbol{v}_g$ is perpendicular to the pressure gradient $\boldsymbol{\nabla_h} p$ and parallel to the isolines of constant pressure (isobars). $\boldsymbol{v}_g$ is proportional to the distance between the isolines.

The geostrophic wind is a good measure for the general wind flow for a given site (area) because of its independence on specific surface characteristics (orography, obstacles, roughness).

Note: The geostrophic approximation is not valid in equatorial regions since the Coriolis force is not defined for $\phi = 0$.

The geostrophic assumption requires the abscence of horizontal accelerations:
$\longrightarrow$ straight steady flow (uncurved flow)
$\longrightarrow$ parallel to isolines of constant pressure
$\longrightarrow v \sim$ distance between isobars

14.4.2 Friction Wind

In the atmospheric boundary layer (ABL) the friction force adds to the acting forces. The balance now is (Fig. 14.3):

$$-\frac{1}{\rho}\boldsymbol{\nabla_h} p - f(\boldsymbol{k} \times \boldsymbol{v}_h) + \mu \boldsymbol{v}_h = 0 \tag{14.22}$$

With decreasing wind velocity the Coriolis force also decreases. To compensate for the pressure gradient force, the wind has to turn left. This indicates that in the

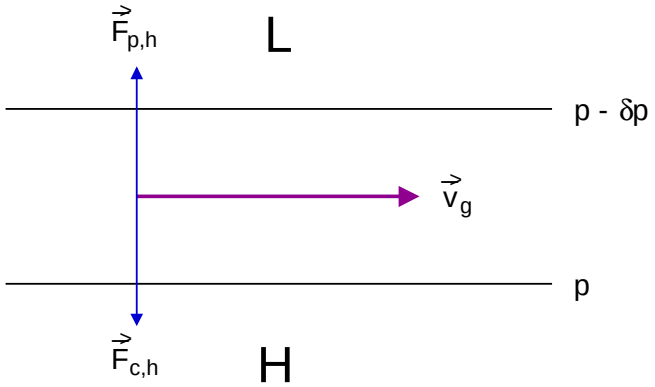

Fig. 14.2. The geostrophic balance. The horizontal components of the pressure gradient force $\boldsymbol{F}_{p,h}$ and the Coriolis force $\boldsymbol{F}_{c,h}$ are balanced. v_g is the geostrophic wind.

atmospheric boundary layer the horizontal wind has a component directed toward lower pressure (Fig. 14.4).

The deflection angle α depends on

– surface roughness
– latitude
– turbulence.

Typical values for the surface wind deflection are 15-30° over sea and 25-50° over land. The corresponding values for v/v_g are 0.8 and 0.5, respectively. Due to the decreasing Coriolis force α increases with decreasing latitude.

The vertical change of wind speed and direction due to the decreasing influence of friction with height is represented by the logarithmic Ekman spiral (Fig. 14.5).

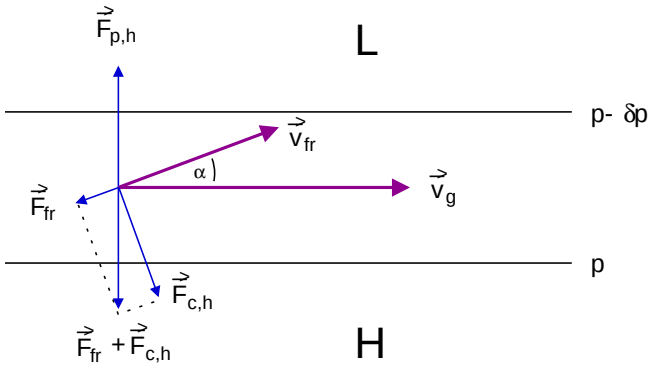

Fig. 14.3. The balance of horizontal forces in the atmospheric boundary layer. The pressure gradient force $\boldsymbol{F}_{p,h}$ is balanced by the sum of the Coriolis force $\boldsymbol{F}_{c,h}$ and the friction force $\boldsymbol{F}_{fr}$.

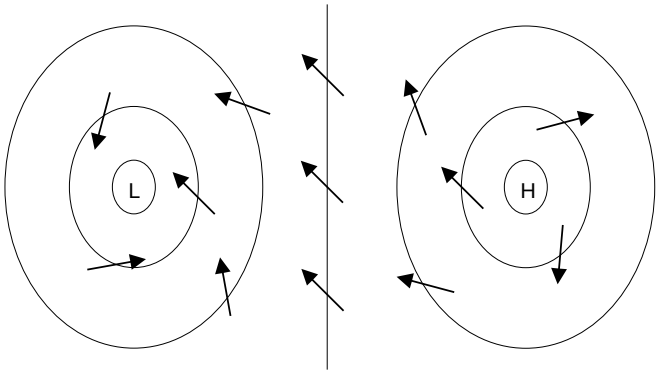

Fig. 14.4. Schematic surface wind pattern associated with centers of high and low pressure. The wind field is indicated by arrows, isobars are shown by solid lines. Note that this holds for the Northern hemisphere only. The circulation in the Southern hemisphere is clockwise for lows and counterclockwise for highs.

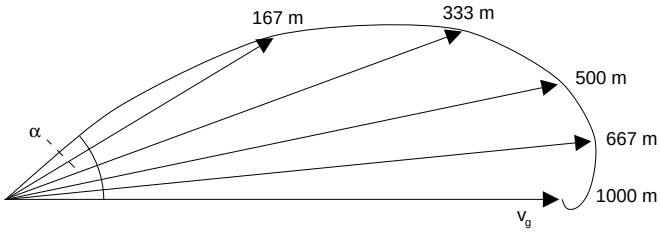

Fig. 14.5. The theoretical Ekman spiral describing the height dependence of the departure of the wind field in the boundary layer from geostrophic balance. α is the directional departure from the geostrophic wind.

15. Wind Climatology

15.1 Local Winds

Establishment of local wind systems by thermally induced pressure gradients.
Driving force: differential heating

The main steps in the development are shown in Fig. 15.1. Note, that for length scales below 100 km the effect of the Coriolis force is small and the air flow follows mainly the pressure gradient.

Examples of local and regional wind systems which are based on this concept:

- sea-breeze winds
- mountain/valley winds
- monsoon winds.

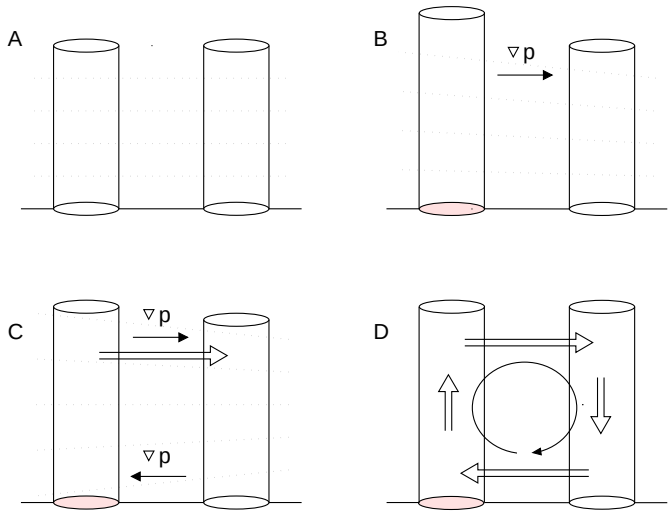

Fig. 15.1. Schematic development of a wind system. **A**. Two columns of air are in hydrostatic equilibrium each. The air is in rest. **B**. Differential heating causes the temperature of the left column to rise and a horizontal pressure gradient between the two columns in larger heights establishes. **C**. This results in a horizontal wind flow directed towards lower pressure and thus produces a horizontal pressure gradient (and a wind flow) at the surface in the opposite direction. **D**. Due to the conservation of mass vertical motion of air is necessary to close the circulation.

15.2 General Circulation of the Atmosphere

(mostly dynamical in nature)
fig.: global circulation
fig.: Hadley circulation
ITCZ: convective clouds
air motion directed towards the equator, by Coriolis force deflection to right
trade winds: east to west (both hemispheres)

Circulation north and south of 30 deg is characterized by strong westerly wind regimes (Rossby circulation).

Separation of tropical air from cold (ant)arctic air masses
$\longrightarrow$ region of strong horizontal contrasts in temperature, pressure, humidity, ...

With this circulation westerly waves are coupled which transport energy from equatorial regions to polar regions.

Year-to-year-variability $\longrightarrow$ wind index

15.3 Wind Resources

Generally, strong wind resources can be expected in regions with permanent (steady) strong wind regimes. That is

- local wind systems (monsoon type)
- orographically induced wind systems
- strong winds resulting from the global circulation (westerlies)

figs.: wind maps

16. Wind Flow in the Atmospheric Boundary Layer

intro: layers of the atmosphere, influence of surface friction

We know: at surface it is: $v = 0$ ms^{-1}.

Above some height h the influence of the surface on the wind flow (through friction, turbulence) can be neglected.

$\longrightarrow$ free atmosphere, geostrophic balanced flow: $v = v_g$

The layer in which the transition between these two states of atmospheric flow occurs is called the *atmospheric boundary layer* (ABL) or planetary boundary layer (PBL).

The properties of the wind flow in the lowest part of the ABL dominate the potential for extracting wind power.

16.1 Boundary Layer Height

considerable variations occur: 100 m $< h <$ 2000 m
Ex.: clear nights and low wind speed: very low
summer day with high insolation: very high

typical value: $h = 1000$ m

The height depends on:

- thermal stability of the atmosphere (daily and annual variability !)
- wind speed
- surface characteristics (roughness, orography, ...)

16.2 Vertical Structure of the Boundary Layer

Transition between $v = 0$ (surface) and $v = v_g$ (top of the ABL) implies strong vertical gradient of wind speed (= wind shear)

$\longrightarrow$ source of turbulence

$\longrightarrow$ vertical fluxes of momentum and heat

The form of the vertical wind speed profile again is strongly influenced by the thermal stability of the atmosphere (which increases or decreases turbulence).

Thermal stability is expressed by means of the actual vertical temperature gradient compared to the adiabatic temperature gradient in dry air ($\Gamma \approx 1$ K / 100 m) for a vertically moving air parcel.

$\partial T/\partial z < 1$ K / 100 m stable
$\partial T/\partial z = 1$ K / 100 m neutral
$\partial T/\partial z > 1$ K / 100 m unstable

The logarithmic wind profile is strictly valid only in a neutrally stratified atmosphere.

Idealizations: horizontal homogeneity and stationarity

Surface layer: assumptions: strong vertical gradients of variables as wind velocity, temperature, ...
$\longrightarrow$ Simple laws analogue to those that govern molecular diffusion in laminar flows might apply for turbulent transport in the lowest atmosphere:

$$\tau = \rho K \frac{\delta \bar{u}}{\delta z}, \tag{16.1}$$

where K is the turbulent exchange coefficient for momentum (the counterpart of viscosity in laminar flows). K is also called the eddy diffusivity or eddy viscosity.

Usually, the atmospheric boundary layer is subdivided in two layers: surface layer, Ekman layer.

16.2.1 The Surface Layer

In heights up to ~ 100 m the shear stress can be approximated to be constant with height (for neutral conditions). Changes in wind direction can be neglected. If the shear stress is written as

$$\tau_{xz} = \rho K \frac{\delta u}{\delta z} \tag{16.2}$$

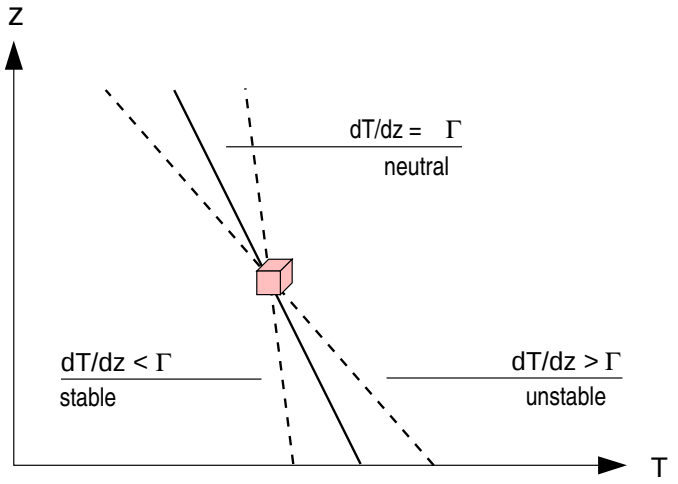

Fig. 16.1. Stability regimes in dry air.

where τ_{xz} represents vertical transport of horizontal momentum and K is the eddy viscosity. This assumption leads to the logarithmic wind profile:

$$\frac{\partial u}{\partial z} = \frac{u_*}{kz} \tag{16.3}$$

where $k \simeq 0.4$ is the von Kármán constant and $u_* = \sqrt{\tau/\rho}$ is the friction velocity, a quantity characterizing the vertical turbulent flux of momentum.

To derive Eq. (16.3), it is used that K can be described in terms of the vertical wind speed gradient and the mixing length l, which represents the length scale necessary for changing the turbulent characteristics of a vertically moving eddy. l also characterizes the size of the eddies involved:

$$K = l^2 \frac{\partial u}{\partial z}, \tag{16.4}$$

where $l = k\,z$.

In its integrated form the logarithmic profile can be written as

$$u(z) = \frac{u_*}{k}\, ln(\frac{z}{z_0}), \tag{16.5}$$

where z_0 is an integration constant denoting the height where $u(z)$ = 0. z_0 can not directly be interpreted as a physical length, but depends on the size and structure of the local roughness elements. For this reason z_0 is called the roughness length. z_0 can experimentally be derived from measured wind profiles, but usually characteristic values for given surface types are used (Tab. 16.2.1).

Table 16.1. Typical values for the roughness length z_o in m.

ice	10^{-5}	high grass	0.04
smooth sea	2-3$\times 10^{-4}$	wheat	0.05
sand	10^{-4} - 10^{-3}	low woods	0.05 - 0.1
grassy surface	0.015 - 0.02	high woods	0.2 - 1.0
low grass, steppe	0.03	suburbia	1 - 2
flat country	0.02	city	1 - 5

Eq. (16.3) and (16.5) are valid only under several assumptions:
- only for mean values (periods longer than 10 min.)
- horizontally homogeneous surface
- neutral stability of the atmosphere

Given a wind speed value in height z_1 and the local roughness length z_0 the complete vertical profile can be calculated using Eq. (16.5):

$$\frac{u(z_1)}{u(z_2)} = \frac{ln(z_1/z_0)}{ln(z_2)(z_0)}. \tag{16.6}$$

Frequently, a simpler power law is used to describe the vertical wind profile:

$$\frac{u(z_1)}{u(z_2)} = (\frac{z_1}{z_2})^{\alpha}, \tag{16.7}$$

where α represents the influence of height, surface roughness and thermal atmospheric stability. An often used value is $\alpha = 1/7$. Due to the strong variability of α the use of the power law is not recommended.

For short period wind speed data ($<$ one hour, instantaneous) the actual atmospheric state (concerning stability) has to be taken into consideration. A commonly used method is the use of the boundary layer similarity theory (Monin-Obukhov theory) by applying a correction function to the logarithmic wind profile:

$$\frac{\partial u}{\partial z} = \frac{u_*}{kz}\,\phi(\frac{z}{L}), \tag{16.8}$$

where $\phi(z/L)$ is a universal function of the height z relative to the similarity scale L (Monin-Obukhov-length). For neutral atmospheres $\phi(z/L) = 1$.

16.2.2 The Ekman Layer

The layer on top of the surface layer characterized by increasing shear stress with height and a changing wind direction with height is called the Ekman layer.

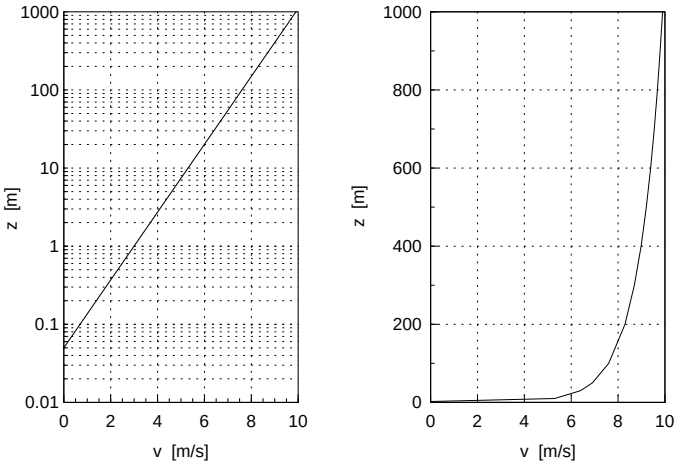

Fig. 16.2. The logarithmic wind profile in logarithmic (left) and linear right) height scale (z_0 = 0.05 m, u^* = 0.4 ms^{-1}).

17. Wind Resource Assessment

17.1 The European Wind Atlas

17.1.1 Overview and Basic Concepts

The European Wind Atlas Analysis and Application Program (WAsP) [24] is since the nineties the standard software tool for the estimation of regional wind power resources.

assessment of wind energy resources:
- establish the meteorological basis for the assessment of wind energy resources
- provide suitable data for evaluating wind power output
- high precision requirements because of $P(v^3)$-dependence
- method need high-quality long time series ($>$ 10 a) of wind data due to long term variations in wind climate

problem:
wind speed at a given site depends on two factors:
- overall weather systems (typical scale: 1000 km)
- nearby topography (typical scale: 10 km)

$\rightarrow$ wind data are representative only valid for the actual position of the station
$\rightarrow$ method for transformation of wind speed statistics is required (horizontal and vertical extrapolation)

$\rightarrow$ solution: European Wind Atlas: set of models based on physical principles of boundary layer flow taking into account:
- effect of different surface conditions (roughness)
- sheltering effects (buildings, trees, ..)
- variations of the terrain height (orography)

$\rightarrow$ three main influences:
- terrain class (surface roughness, four classes)
- sheltering obstacles
- terrain height variations (orography)

regional wind climatologies have been calculated from more than 200 sites (at least 10 a of data and accurate site descriptions each)

calculation of generalized wind climate:
- flat and homogeneous terrain
- no nearby obstacles

- heights of 10, 25, 50, 100, 200 m - four roughness classes → 20 data sets free from local influences → regionally representative

spatial scale of representativeness depends on orographic structure of landscape:
- flat, open terrain: up to 200 km
- mountainous area: close to station

regional data sets mainly give statistical information in terms of the probability distribution function (this is sufficient information foe wind power estimates) → use of Weibull distribution division into 12 wind direction classes → 240 sets of Weibull parameters

essential: systematic description of topographic characteristics: - effects of obstacles → sheltering effects
- surface of terrain
- topographic elements contributing to roughness: vegetation, houses
- orographic influence: decrease/increase of wind speed due to hills, ridges, cliffs, ..

→ three main effects of topography:
- shelter
- roughness
- orography

17.1.2 Physical Models

logarithmic profile: $u(z) = \frac{u_*}{\kappa} \ln(\frac{z}{z_0}) - \Psi(\frac{z}{L})$

geostrophic drag law: $u_g = \frac{u_*}{\kappa}\sqrt{((\ln(\frac{u_*}{f z_0}) - A)^2 + B^2)}$

assumptions: stationarity, homogeneity, barotrophy, neutral stability

→ balance geostrophy and surface roughness

stability corrections:
- small wind speeds not important → neutral assumption generally good
- modifications as small perturbations to neutral state
- input: climatological average, variance of surface heat flux

→ effect on vertical profiles of climatological means and standard deviations of wind speeds
taking average values for overland and sea stations, respectively

Surface Roughness. roughness is determined by size and distribution of roughness elements
Wind Atlas includes four types: → roughness classes
roughness parameterized by length scale z_o
empirical relationship with size of elements: $z_0 = 0.5hS/A_H$ with height h, cross sectional area S and density A_H (average horizontal area occupied by each element)
porosity for non-solid elements!

seasonal changes of roughness!

Shelter Effects by Obstacles. shelter effect: relative decrease in wind speed behind an obstacle

depending on:
- distance from obstacle to site

- height of obstacle
- height at site (rotor hub height)
- length of obstacle (lateral → infinite: max. shelter, zero: no shelter)
- porosity of obstacle ($\simeq 0$ for buildings, ~ 0.5 for trees (changing seasonally), $\sim$ 0.33 for row of buildings with spacings of 1/3 the building length between them

Orographic Effects. Example: flow over Askervein hill (Hebride islands); length scale: 1 km

results: speed increases by a factor of 1.8 on top of the hill; negative speed-up in front and lee of the hill (20-40 percent)

for moderate orography simple corrections for these effects can be applied

for complicated terrain numerical hydrodynamical models have to be used

17.1.3 Application of the Model

Step 1: Select a base station

→ regional wind climatology (one of the available Wind Atlas sites, i.e. statistical description)

requirement: similar topographic situation; distance usually < 100 km;

mountains, coastlines!

Step 2: Roughness description

classifying surface types around the site

→ division into 12 $30\,\mathrm{deg}$-sectors and sector-by-sector classification (roughness classes)

→ Weibull distribution for each sector

roughness description with changes in a given sector (roughness change):

→ non-homogeneous surface → problem: defining a unique roughness length

→ development of internal boundary layer with height h and distance from roughness change x:

$\frac{h}{z_0}(ln(\frac{h}{z_0}-1)) = const\frac{x}{z_0}$

$z_0 = max(z_{01}, z_{02})$

→ modelling new profile with several logarithmic parts

→ correction factor for Weibull A parameter: $A = corrA_{upwind}$

$corr = \frac{\ln(z/z_{o2})\ln(h/z_{o1}}{\ln(z/z_{o1})\ln(h/z_{o2}}$

with height h of internal boundary layer

→ dividing segment into parts with equal roughness

Step 3: Calculation of total Weibull distribution

- A,k for each sector available; also the relative frequencies of occurrence
- calculation of mean M_i and mean squares u_i^2 for each sector
- calculate total mean and mean square
- from M^2/u^2 calculate k
- use table to calculate u

$M = A\Gamma(1+\frac{1}{k})$

$u^2 = A^2\Gamma(1+\frac{2}{k})$

$\frac{M^2}{u^2} = \frac{\Gamma^2(1+\frac{1}{k})}{\Gamma(1+\frac{2}{k})}$
- note: assumption: total distribution is Weibull distribution
Step 4: Shelter effects
Correction of Weibull A parameter depending on: - distance obstacle-site (x)
- height and length of obstacle (h, L)
- height at site (H)
- porosity of obstacle (P)
→ empirical relationships
Step 4: Orography
Correction for speed-up effects from local terrain inhomogeneities
Assumption: flow is modelled as potential flow
→ velocity is gradient of a potential $\boldsymbol{u} = \nabla\chi$
→ calculation of potential flow perturbations by terrain
advantage: mathematically attractive description (polar representation)
→ potential flow perturbation
→ surface friction effects
$A_{corr} = A(1 + \Delta S)$
$\Delta S = f(H.L)$ with half width L and height H
for smooth hills (slope $<\approx$ 0.3) only!

17.2 Resource Assessment in Complex Terrain - Mesoscale Modelling

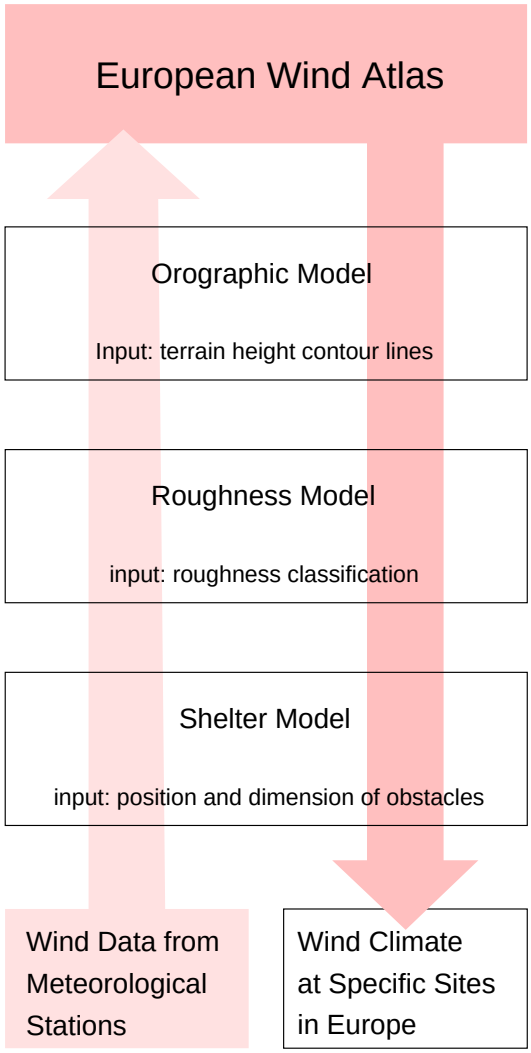

Fig. 17.1. Structure of the Wind Atlas Analysis and Application Program.

18. Wind Power Modelling

chapters on:

- WAsP
- mesoscale models
- wake models
- wind farm models
- advanced (research) techniques
- remote sensing techniques (offshore)
- instrumentation and operation of a met tower
- standardization (IEC, ..)

18.1 ....

18.1.1 .....

19. Wind Measurements

chapters on:

- standard anemometry
- ultrasonic anemometer
- SODAR
- advanced (research) techniques
- remote sensing techniques (offshore)
- instrumentation and operation of a met tower
- standardization (IEC, ..)

20. Offshore Wind Power

20.1 ....

20.1.1 .....

21. Wind Power Forecasting

21.1 ....

21.1.1 .....

Part III

Appendix

A. Statistical Characterization of Meteorological Time Series

A.1 Time Series: Mean and Variance

The values of meteorological variables typically change with time.

Measurements of these variables: Recording the instantaneous (i.e. discrete) values for moments with a constant (equidistant) time step Δt:

Examples: Weather observations every 3 or 6 hours, digital data recording systems with measurement frequencies below 1 Hz;

The sequence of data gained from these measurements $\{x_{t_1}, x_{t_2}, x_{t_3}, \ldots, x_{t_n}\}$ is called a *time series*.

The frequency of change (fluctuation) in a given time series changes itself with time and is a priori not known. Excepting the well known daily and annual cycles these fluctuations are partly due to the evolving weather condition (e.g. moving cyclones) and to statistically distributed perturbations (wind turbulence, irradiance influenced by moving clouds). Fluctuations are usually different for different variables and for different time scales.

$\longrightarrow$ The time series usually contain both, deterministic and stochastic components.

The maximum frequency that can be measured is determined by:

– response of the measuring instrument (time constant), example: thermal pyranometer vs. solar cell pyranometer

– sanmpling rate of data aquisition system.

The *sampling theorem* states that the sampling rate must have a minimum time interval of $1/2B$ (Nyquist-interval), where B is the bandwidth.

The value $x(t_i)$ then represents the quality x for the period between $(t_i - \Delta t/2$ and $t_i + \Delta t/2)$. $x(t_i)$ is assumed as the mean value of x for this period.

Assuming n instantaneous measurements of the variable x with a constant time interval Δt. Then the *mean value* of the total time period T is given by

$$\bar{x} = \frac{1}{n} \sum_{i=1}^{n} x(t_i). \tag{A.1}$$

This is an approximation for the exact mean value given by

$$\bar{x} = \frac{1}{T} \int_0^T x(t) dt. \tag{A.2}$$

Mean values do not contain any information about the deviation of the time series values from this value. A measure for the deviation from the mean is given by the *variance* of $x(t)$:

$$\sigma^2 = \frac{1}{n}\sum_{i=1}^{N}\left(x(t_i) - \bar{x}\right)^2 = \overline{x^2} - \bar{x}^2. \tag{A.3}$$

σ is called the *standard deviation* and is a measure of the deviation from the mean which possesses the same unit as the variable under consideration.

A.2 Frequency Distributions

Typically, not only the time scale is divided into discrete time steps but also the range of values is seperated into classes. As an example, Table A.2 lists results from a wind classifier.

Table A.1. Separation of wind speed time series values in classes with width of 1 m/s.

no. of class	lower limit	upper limit	no. of values in class		
j	$x_l(j)$	$x_u(j)$	$n(j)$	$h(j)$	$H(j)$
1	0.0	0.99	30	0.15	0.15
2	1.0	1.99	60	0.30	0.45
3	2.0	2.99	50	0.25	0.70
4	3.0	3.99	30	0.15	0.85
5	4.0	4.99	20	0.10	0.95
6	5.0	5.99	10	0.05	1.00

N=200

The graphical representation of the frequency distribution is the histogram in Fig A.1. The relative frequency (or the probability) that the values $x(t_i)$ fall into class j is

$$h_j = \frac{n(j)}{N}. \tag{A.4}$$

Note that the relative frequencies can only be interpreted as probabilities if the sample size is large enough so that mean and variance of both sample and total 'population' are equal!

An alternative presentation of the same information is the cumulative probability diagram also shown in Fig. A.1. The cumulative probability is given by

$$Hj = \sum_{k=1}^{j} h(k) \tag{A.5}$$

and gives the frequency of occurrence of classes below a value x_j.

When connecting the upper right points of the bars in the cumulative probability diagram, a function F which is piecewise linear is given. The gradient of F in a given class is

$$\frac{F(x_u(2)) - F(x_l(2))}{x_u(2) - x_l(2)} = \frac{\Delta F}{\Delta x} = f \tag{A.6}$$

or

$$f(j) = \frac{H(j) - H(j-1)}{\Delta x}. \tag{A.7}$$

f is called the *probability density*.

Note: $f \neq$ relative probability! The relative probability gives the probability for being in a given class (independent on its width). The probability density is normalized by the class width. For wind speed data, f has the dimension $(\mathrm{m/s})^{-1}$.

The smaller the class width, the more the cumulative probability curve approximates to an continuous curve. For an infinitesimal small class width δx F becomes a continuous distribution function of x: $F(x)$.

The probability density f then is

$$f_x = \frac{dF(x)}{dx} \tag{A.8}$$

or:

$$F_x = \int_{x_{min}}^{x} f(x)dx. \tag{A.9}$$

For f the following conditions apply:

$$0 \leq f(x) \leq 1 \qquad \text{for all } x, \tag{A.10}$$

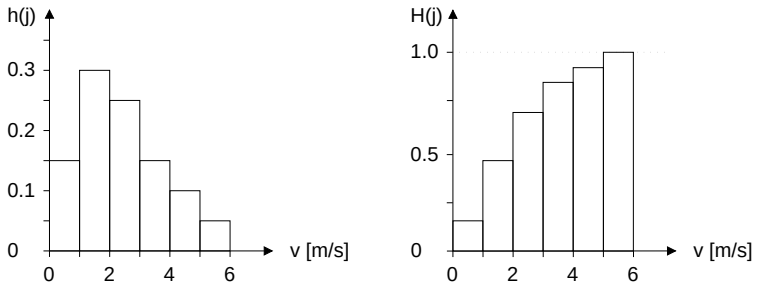

Fig. A.1. Histograms of the relative frequency (left) and the cumulative frequency (right) for the wind speed values given in Table A.2.

$$\int_{x_{min}}^{x_{max}} f(x)dx = 1. \tag{A.11}$$

The relative probabilities $h(j)$ for a given class width $\delta x = x_u - x_l$ is

$$h(j) = \int_{x_l(j)}^{x_u(j)} f(x)dx = F(x_u(j) - F(x_l(j)). \tag{A.12}$$

$\longrightarrow$ The relative probability for a given class width can be reconstructed from f or F.

A.3 Examples of Analytical Probability Distributions

A.3.1 Normal Distribution

A most often used probability distribution is the Gaussian or normal distribution (Fig. A.2) with the probability density

$$f_g = \frac{1}{\sqrt{\sigma 2\pi}}\, e^{-\frac{(x-\bar{x})^2}{2\sigma^2}}, \qquad \sigma \geq 0,\ -\infty < x < +\infty \tag{A.13}$$

and the corresponding distribution function

$$F_g = \frac{1}{\sqrt{\sigma 2\pi}} \int_{-\infty}^{x} e^{-\frac{(x-\bar{x})^2}{2\sigma^2}} dx. \tag{A.14}$$

which gives the cumulative distribution. The Gaussian distribution is commonly applied to describe the statistical errors in the process of repeated measurements of the same quantity ($\rightarrow$ law of large numbers). It is symmetric with respect to the mean $\bar{x}$. The probability that a measured value lies in the range $[\bar{x} - \sigma, \bar{x} + \sigma]$ is 0.682.

The Gaussian distribution is an appropriate approximation of the variation of short time wind speed data ($\delta t \approx 1$ s) around their hourly mean value. Unfortunately, it cannot be applied to the distribution of hourly wind speed data for longer periods (e.g. one year).

A.3.2 Weibull Distribution

For wind speed data, the Weibull distribution has shown to be a good approximation of the real data set. Its functional representations are:

$$f_w(x) = \frac{k}{A}\,(\frac{x}{A})^{k-1}\, e^{-(x/A)^k} \tag{A.15}$$

and

$$F_w(x) = e^{-(x/A)^k}, \tag{A.16}$$

where the *shape factor* k usually is close to 2.0 and the *scaling factor* A is close to the mean wind speed. For a constant shape factor k = 2 the distribution is called *Rayleigh distribution*.

Plots: different Weibull distributions

It can be shown that the Weibull parameter k and c are related to the mean $\bar{x}$ and the variance σ^2 of the time series:

$$\bar{x} = A\,\Gamma(1 + \frac{1}{k}) \tag{A.17}$$

and

$$\sigma^2 = A^2 \left(\Gamma(1 + \frac{2}{k}) - \left(\Gamma(1 + \frac{1}{k})\right)^2\right), \tag{A.18}$$

where Γ is the Gamma function defined by

$$Gamma(x) = \int_0^\infty t^{x-1}\, e^{-t}\, dt. \tag{A.19}$$

A measure of the variation of the time series around the mean value is the quantity $\sigma/\bar{x}$ (coefficient of variation), which only is a function of the shape parameter k:

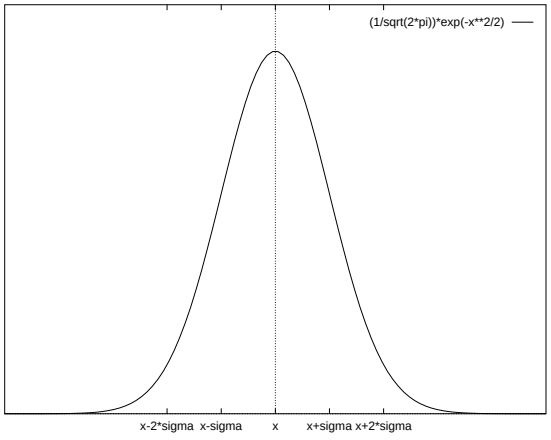

Fig. A.2. Probability density function for the Gaussian distribution.

$$\frac{\sigma}{\bar{x}} = \frac{\sqrt{\Gamma(1+\frac{2}{k}) - (\Gamma(1+\frac{1}{k}))^2}}{\Gamma(1+\frac{1}{k})}. \tag{A.20}$$

For use in relationship with wind energy a nice behavior of the Weibull distribution is the ability to directly calculate the mean cube of the variable x:

$$\bar{x^3} = A^3\ \Gamma(1+\frac{3}{k}). \tag{A.21}$$

The calculation of the Weibull parameters for a measured time series can be done in the following manner:
1. Calculate the mean $\bar{x}$ and the standard deviation σ of the time series.
2. With $\sigma/\bar{x}$ find k from table A.3.2.
3. With k and $\bar{x}$ find A with Eq. ... and tabulated Γ-function values. [1]

A.4 Autocorrelation

[1] Γ-function tables can be found in mathematical tables (e.g., *Bronstein: Taschenbuch der Mathematik*).

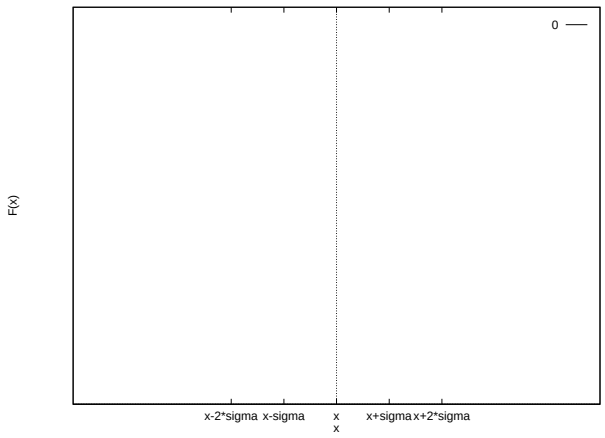

Fig. A.3. umulative probability function for the Gaussian distribution.

Table A.2. Weibull shape parameter k as a function of $\sigma/\bar{x}$.

k	$\sigma/\bar{x}$	k	$\sigma/\bar{x}$
1.2	0.837	3.0	0.363
1.4	0.742	3.5	0.316
1.6	0.640	4.0	0.281
1.8	0.575	5.0	0.229
2.0	0.523	6.0	0.194
2.2	0.480	7.0	0.168
2.4	0.444	8.0	0.148
2.6	0.413	9.0	0.133
2.8	0.387	10.0	0.120

B. Unit Sphere and Solid Angle

Any point within a cartesian frame of reference may be indicated by the position vector $\boldsymbol{r}$ such that

$$\boldsymbol{r} = (x, y, z) \tag{B.1}$$

where (x, y, z) defines the coordinates of the tip of the vector. A direction vector in terms of a unit position vector $\boldsymbol{\xi}$ which has its base at the origin and tip at the point (a, b, c) where this point lies on the unit sphere that surrounds the origin. In this case $\sqrt{a^2 + b^2 + c^2} = 1$. A trigonometric interpretation of the direction vector is

$$\begin{aligned} a &= \cos\phi \sin\theta \\ b &= \sin\phi \sin\theta \\ c &= \cos\theta \end{aligned} \tag{B.2}$$

where θ is the zenith angle and ϕ is the azimuth angle. The direction vector then is

$$\boldsymbol{\xi} = (\cos\phi \sin\theta, \sin\phi \sin\theta, \cos\theta). \tag{B.3}$$

Many radiation problems require the consideration of radiant energy confined to an element of solid angle. A convenient way to think about the solid angle is to imagine a point source of light located at the center of a unit sphere. A small hole of area A on the surface of the sphere allows light to flow through it. This light is contained in a small cone of directions which is represented by the solid angle element

$$\Omega = \frac{A}{r^2} \tag{B.4}$$

where r is the radius of the sphere. Given a unit sphere (i.e., r = 1) the area of the opening is

$$r^2\Omega = r^2 \int_A d\Omega = r^2 \int\int_A dadb = r^2 \int\int_A \sin\theta d\theta d\phi. \tag{B.5}$$

Since r = 1, the solid angle element $d\Omega$, which has units of steradian (sr), is related to θ and ϕ according to

$$d\Omega = \sin\theta d\theta d\phi. \tag{B.6}$$

The solid angle associated with all directions around a sphere has the same value in steradians as the surface area of a unit sphere, namely 4π.

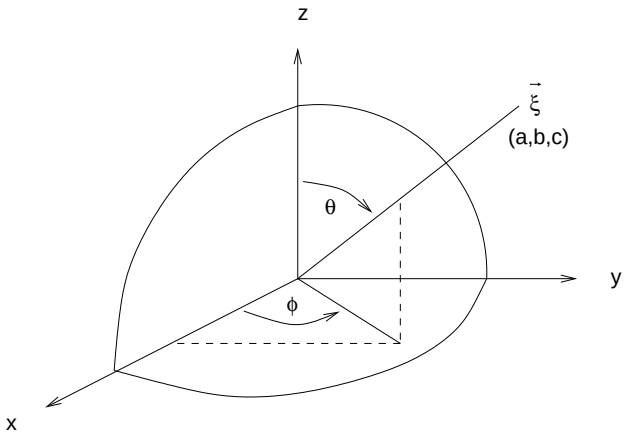

Fig. B.1. Angle and direction definitions defined with respect to a unit sphere.

C. Physical Constants and Data

Table C.1. Physical constants

c = 2.9979 $\times$ 10^{8} ms^{-1}	Speed of light in vacuum
h = 6.6261 $\times$ 10^{-34} Js	Planck's constant
k = 1.38065 $\times$ 10^{-23} JK^{-1}	Boltzmann constant
σ = 5.6704 $\times$ 10^{-8} Wm^{-2}K^{-4}	Stefan-Boltzmann constant
r_s = 6.9600 $\times$ 10^{8} m	Mean radius of the sun
r_e = 6.371 $\times$ 10^{6} m	Mean radius of the earth
m_e = 5.988 $\times$ 10^{24} kg	Mass of the earth
r_{ES} = 1.4960 $\times$ 10^{11} m	Mean distance between earth and sun
Ω = 7.292 $\times$ 10^{-5} rads^{-1}	Earth's angular speed of rotation
g = 9.80665 ms^{-1}	Acceleration of gravity at sea level and 45 $^\circ$ latitude
c_v = 717 JK^{-1}kg^{-1}	Specific heat of dry air at constant volume
c_p = 1004 JK^{-1}kg^{-1}	Specific heat of dry air at constant pressure
R = 287 JK^{-1}kg^{-1}	Gas constant for dry air
p_0 = 1013.25 hPa	Standard sea-level pressure
T_0 = 288.15 K	Standard sea-level temperature
ρ_0 = 1.225 kgm^{-3}	Standard sea-level density of dry air
λ_0 = 1.239 μm	wavelength in vacuum associated with photon energy of 1 eV

Table C.2. Conversion factors – Energy density

Units	Jm^{-2}	Whm^{-2}	calcm^{-2}
1 Jm^{-2}	1	2.778 $\times$ 10^{-4}	2.388$\times$$10^{-5}$
1 Whm^{-2}	3.6 $\times$ 10^{3}	1	0.08598
1 calcm^{-2}	4.187 $\times$ 10^{4}	11.63	1

A *flux* is the rate at which a substance flows. The energy flux indicates the amount of energy [J] that flows in a unit of time [s]. Its unit is Watt [W].

Fluxes therefore are only defined in an instantaneous sense. Often it is more convenient to operate with values which are integrated over a certain time interval (e.g., an hour, a day) and we have to deal with energy densities. In this case, in solar energy, usually the suffix ance is replaced by the suffix ation

Table C.3. Basic radiometric quantities

Quantity	Symbol	Unit
wavelength	λ	m, μm
frequency ($\nu = c/\lambda$)	ν	s^{-1}
wavenumber ($k = 1/\lambda$)	k	m^{-1}, cm^{-1}
radiant energy	Q	J = Ws
radiant flux	Φ	W
radiant flux density (general)	M, E	Wm^{-2}
irradiance (incident onto a surface)	E	Wm^{-2}
radiant exitance, emittance (emerging from a surface)	M	Wm^{-2}
solar radiant flux density (global irradiance)	$E_g^{\downarrow}, G$	Wm^{-2}
radiance, radiant intensity (radiant flux propagating in a given direction within a solid angle)	L, I	$Wm^{-2}sr^{-1}$
insolation		
generic term representing the solar energy received on a horizontal surface whatever the time interval considered		
in specific cases it is replaced by:		
irradiance: instantaneous insolation		Wm^{-2}
irradiation: integrated irradiance over a specific time period (usually: one hour, one day)		Jm^{-2}

References

General

1. J.P. Peixoto, A.H. Oort: *Physics of Climate* (American Institute of Physics, New York, 1992)
2. M.L. Salby: *Fundamentals of Atmospheric Physics* (Academic Press, 1996)
3. C.-D. Schönwiese: *Klimatologie* (Ulmer, Stuttgart, 1994)
4. T. Twidell, T. Weir: *Renewable Energy Resources* (E&FN Spon UK, 1986).
5. J.M. Wallace, P. V. Hobbs: *Atmospheric Science. An Introductory Survey*. Academic Press, New York, 1977)
6. World Meteorological Organization: *Guide to Meteorological Instruments and Methods of Observation*, 5th edn. (WMO No. 8, Geneva, 1983)

Solar Radiation

7. K.L. Coulson: *Solar and Terrestrial Physics* (Academic Press, 1975)
8. J.A. Duffie, W.A. Beckman: *Solar Engineering of Thermal Processes*, 2nd edn. (Wiley & Sons, 1991)
9. R. Festa, C.F. Ratto: *Solar Radiation Statistical Properties*. (IEA Solar Heating and Cooling Programme Task 9 Subtask E. Technical Report No. IEA-SHCP-9E-4, 1993)
10. J.E. Hay, D.C. McKay: 'Estimating solar irradiance on inclined surfaces: A review and assessment of methodologies'. Int. J. Solar Energy **3**, 203-240 (1985)
11. M. Iqbal: *An Introduction to Solar Radiation* (Academic Press, Toronto, 1983)
12. S. Q. Kidder, T. H. Vonder Haar: *Satellite Meteorology: An Introduction* (Acdemic Press, San Diego, 1995)
13. K.-N. Liou: *An Introduction to Atmospheric Radiation* (Acdemic Press, Orlando, 1980)
14. W. Palz, J. Greif (Eds.): *European Solar Radiation Atlas*, 3rd edn. (Springer, Berlin, 1996)
15. E. Raschke, R. Stuhlmann, W. Palz, T.C. Steemers: *Solar Radiation Atlas of Africa* (Balkema, Rotterdam, 1991)
16. M.R. Riches (Ed.): *An Introduction to Meteorological Measurements and Data Handling for Solar Energy Applications* (U. S. Dept. of Energy, DOE/ER-0084, 1980)
17. N. Robinson (Ed.): *Solar Radiation* (Elsevier, Amsterdam, 1966)
18. J.W. Spencer: 'Fourier series representation of the position of the sun'. Search **2**, 172 (1971)
19. World Meteorological Organization: *Meteorological Aspects of the Utilization of Solar Radiation as an Energy Source*. (WMO No. 557, Technical Note No. 172, Geneva, 1981)

Wind Energy

20. W.F. Hughes and J.A. Brighton: *Schaum's Outline of Theory and Problems of Fluid Dynamics* (McGraw Hill, 1991)
21. C.G. Justus: *Winds and Wind System Performance* (Franklin Institute Press, Philadelphia, 1978)
22. D.P. Lalas and C.F. Ratto (Eds.): *Modelling of Atmospheric Flow Fields* (World Scientific, Singapore, 1996)
23. E.H. Lysen: *Introduction to Wind Energy* (SWD Steering Commitee Wind Energy Developing Countries, Amersfoort, The Netherlands, 1982)
24. Troen, I. and E.L. Peterson, : *European Wind Atlas* (Riso National Laboratory, Roskilde, Denmark, 1989)
25. E. Plate (Ed.): *Engineering Meteorology* (Elsevier, 1982)
26. R.B. Stull: *An Introduction to Boundary Layer Meteorology* (Kluwer Academic, 1988)
27. World Meteorological Organization: *Meteorological Aspects of the Utilization of Wind as an Energy Source* (WMO No. 575, Technical Note No. 175, Geneva, 1981)